General Disclaimer

One or more of the Following Statements may affect this Document

- This document has been reproduced from the best copy furnished by the organizational source. It is being released in the interest of making available as much information as possible.

- This document may contain data, which exceeds the sheet parameters. It was furnished in this condition by the organizational source and is the best copy available.

- This document may contain tone-on-tone or color graphs, charts and/or pictures, which have been reproduced in black and white.

- This document is paginated as submitted by the original source.

- Portions of this document are not fully legible due to the historical nature of some of the material. However, it is the best reproduction available from the original submission.

DEPARTMENT OF CHEMICAL SCIENCES
SCHOOL OF SCIENCES AND HEALTH PROFESSIONS
OLD DOMINION UNIVERSITY
NORFOLK, VIRGINIA 3508

(NASA-CR-176075) QUASI N-INTRUSIVE SAMPLING AND ANALYSIS OSES ASSOCIATED WITH THE BOUNDARY LAYE N THE TETHERED SATELLITE AND SIMILAR SCNIC AND HYPERSONIC RESEARCH (Old Dominion Univ., N85-31140

Unclas G3/18 15726

QUASI NON-INTRUSIVE SAMPLING AND ANALYSIS OF GASES ASSOCIATED WITH THE BOUNDARY LAYER ON THE TETHERED SATELLITE AND SIMILAR SUPERSONIC AND HYPERSONIC RESEARCH VEHICLES

By

Charles Fishel, Stacie Niederriter

and

Kenneth G. Brown, Principal Investigator

Final Report
For the period May 1, 1984 through April 30, 1985

Prepared for the
National Aeronautics and Space Administration
Langley Research Center
Hampton, Virginia 23665

Under
Master Contract NAS1-17099
Task Authorization No. 35
Dr. George M. Wood Jr., Technical Monitor
IRD-General Research Instrumentation Branch

June 1985

DEPARTMENT OF CHEMICAL SCIENCES
SCHOOL OF SCIENCES AND HEALTH PROFESSIONS
OLD DOMINION UNIVERSITY
NORFOLK, VIRGINIA 23508

QUASI NON-INTRUSIVE SAMPLING AND ANALYSIS OF GASES ASSOCIATED WITH THE BOUNDARY LAYER ON THE TETHERED SATELLITE AND SIMILAR SUPERSONIC AND HYPERSONIC RESEARCH VEHICLES

By

Charles Fishel, Stacie Niederriter

and

Kenneth G. Brown, Principal Investigator

Final Report
For the period May 1, 1984 tnrougn April 30, 1985

Prepared for the
National Aeronautics and Space Administration
Langley Research Center
Hampton, Virginia 23665

Under
Master Contract NAS1-17099
Task Authorization No. 35
Dr. George M. Wood Jr., Technical Monitor
IRD-General Research Instrumentation Branch

Submitted by the
Old Dominion University Research Foundation
P. O. Box 6369
Norfolk, Virginia 23508

June 1985

TABLE OF CONTENTS

LIST OF TABLES

LIST OF FIGURES

LIST OF FIGURES - Continued

LIST OF FIGURES - Continued

LIST OF FIGURES - Concluded

LIST OF SYMBOLS

A	Cross sectional area
Ar	Argon
C_D	Discharge coefficient
CO_2	Carbon dioxide
d	Diameter of capillary
GADS	Gas Analysis and Detection System
He	Helium
I	Intensity of a mass peak
Kn	Knudsen number
k	Clausing constant
L	Length of capillary
M	Molecular weight
MCP	Multichannel plate
MS	Mass spectrometer
$\dot{m}$	Mass flow
N	Nitrogen atom
N_2	Nitrogen
Ne	Neon
NO	Nitric Oxide
O	Oxygen atom
O_2	Oxygen molecule
P	Pressure
ΔP	Pressure drop across the multichannel plate
Q	Volume flow
R	Gas constant
Re	Reynolds constant

r	Radius of the capillary
T	Temperature (K)
v	Vehicle velocity
$\bar{v}$	Average molecular velocity
x	Nondimensional shuttle x coordinate
X_N	Mole fraction of species N
y	Nondimensional y coordinate
Y	Distance from the surface
Y_{bl}	Boundary layer thickness

Greek Symbols

γ	Specific heat ratio
ϵ	Transparency of MCP
σ	Molecular diameter
λ	Mean free path
μ	Viscosity
ρ	Density
ρ_N	Number density

Subscripts

1	upstream
2	downstream
bl	at the boundary layer edge
GL	at the mass spectrometer inlet
isen	isentropic
meas	measured

QUASI NON-INTRUSIVE SAMPLING AND ANALYSIS OF GASES ASSOCIATED WITH THE BOUNDARY LAYER ON THE TETHERED SATELLITE AND SIMILAR SUPERSONIC AND HYPERSONIC RESEARCH VEHICLES

By

Charles Fishel,[1] Stacie Niederriter,[2] Kenneth G. Brown[3]

INTRODUCTION

The mass spectrometric analysis of the environment surrounding an object such as a reentry vehicle or a low earth orbit satellite requires the removal of some of the atmosphere present at the surface of the object. It is necessary that the sample removal be as non-intrusive as possible since there will be other instrument packages on the vehicle, some downstream of the sampling site. The opening in the surface of the vehicle, acting as an inlet to the mass spectrometer, should either have no effect upon the composition of the sample or any affect that might occur should be well-characterized beforehand under the physical conditions that a test object might encounter upon reentry or in earth orbit.

This report considers the effect that one candidate inlet, an assembly of capillary openings in a thin glass plate (a multichannel plate), might have on the overall sampling process. The flow characteristics of the plate, under a variety of conditions of external pressure and mass flow, will be evaluated. The first part of the report is a review of capillary flow theory with some development of the pertinent equations. The predicted

---

[1]Research Technician, Chemical Sciences Department, Old Dominion University, Norfolk, Virginia 23508

[2]Undergraduate Research Assistant, Chemical Sciences Department, Old Dominion University, Norfolk, Virginia 24508

[3]Associate Professor, Chemical Sciences Department, Old Dominion University, Norfolk, Virginia 23508.

mass flow will be compared to that determined experimentally to assess the effect that mass flow through one capillary might have upon a neighboring capillary. The second section of the report is concerned with mass spectrometric measurements of gas mixtures flowing through the multichannel plate (MCP). In the first part of the experiments, the flow was in a direction normal to the surface of the plate. The experimental gases were Argon and mixtures of carbon dioxide in air. The resultant ratios of carbon dioxide to nitrogen and oxygen were determined and compared with the original sample to determine when separation by molecular weight occurred. In the third section, ongoing experiments are discussed which are conducted with the flow parallel to the surface of the plate, a simulation of the kind of flow that a flight vehicle would experience. We are initially interested in determining the pressure drops that will occur across the plate as the external pressure is varied, and the resultant flow rates that will be attained. Eventually the mass separation that will occur, at the inlet, as the pressure is lowered will also be determined. The fourth section of the report summarizes the results of calculations which attempt to emulate the expected environment at the surface of a reentry vehicle as it descends. The physical conditions that would exist at the surface of the vehicle and in the boundary layer are predicted. In addition, the gas composition at the surface and in the boundary layer will be estimated assuming that the only species present are N atom, O atom, O_2, N_2, and NO.

EXPERIMENTAL

In the first set of experiments a multichannel plate fashioned from leaded glass and furnished by Galileo Electro-optics was used as the model effusive inlet. A magnified view of the MCP with an accompanying reference

scale in units of .01 mm is shown in Figure 1. The holes were determined to average 9.6 μm in diameter with the plate having a thickness of 400 μm. There are, in this particular plate, 7.48×10^4 holes/cm^2 resulting in approximately 58% "empty space" in the plate. For the experiment, the plate was mounted on a Teflon mask which had a hole in its center of approximately 1.6 mm in diameter. The Teflon mask reduced the effective open area of the MCP and provided a seal to ensure that no gas leaked around the MCP. The plate and mask were held in a flange with the whole assembly being connected to the experimental apparatus represented schematically in Figure 2. In all of the experiments described in this section, the gas flow was normal to the surface of the plate. The pressure drop, ΔP, across the flange, and thusly across the MCP, the upstream pressure, P_1, and the pressure at the gold leak inlet to the mass spectrometer, P_{GL}, were monitored by barocel pressure transducers. The mass flow $\dot{m}$ was monitored by Haystings mass flow meters with flow ranges of either 0-20 or 0-100 sccm/min. All flows were corrected for actual conditions of pressure, temperature and nature of the gas. The flow in the system was established with the use of a mechanical forepump connected to the line in front of the gold leak entrance to the mass spectrometer. In addition, the sample was pumped through the gold leak using another mechanical forepump and the ion pump on the mass spectrometer. The mass spectrometer was calibrated for the particular gas involved in this experiment by direct injection of a sample of a gas of known concentration into the mass spectrometer ion source.

The net effect of the multichannel plate, or effusive inlet, upon the flow can be seen in Figure 3. The measurements in Figure 3 were made with the apparatus shown in Figure 2 with the mask, by itself, in the flange and with the mask and effusive inlet in the flange. At higher pressures the

multichannel plate produces a considerable pressure drop, although the downstream pressure, P_2, is still relatively large. For example, at an applied pressure of 20 torr the pressure drop is 15 torr resulting in a downstream pressure of 5 torr which would be too large for a mass spectrometer ion source. As the applied pressure is lowered, the pressure drop falls precipitously. An extrapolation would indicate that at low pressure, although still unreasonably high for a typical MS ion source, P_1 and P_2 would become approximately equal, indicating that this particular plate is not a barrier for the gas. It should be emphasized here that this is data from one plate with a particular hole density and length. The concept of the plate itself is promising and with some modification, particularly in hole density, would produce pressure drops that would enable the operation of the mass spectrometer over a variety of pressure ranges. Such modifications are currently under study. The effect of capillary size upon the composition and physical nature of the flow will also be evaluated.

Figures 4 and 5 show the effect of the upstream to downstream pressure ratio on the flow through the multichannel plate in comparison with an empty flange. For both the case of pure Argon (Ar) and 15% CO_2 in air, the flow reached a maximum at a P_1/P_2 of about 3. For both gases the flow through the MCP attains a plateau at a flow rate that is approximately 50% lower than the empty flange case. The extent of flow reduction is a consequence of the plate having approximately 58% free space, as stated earlier. In both experiments the upstream pressure, P_1, was 4 torr.

The downstream pressure as a function of mass flow is shown in Figures 6 and 7. Again the applied pressure was 4 torr. As P_2 decreases mass discrimination effects begin to appear. At low P_2 the extrapolated flow is higher in the 15% CO_2 in air mixture than for pure Ar.

The effect of the multichannel plate on the composition of a given sample was determined using a mass spectrometer developed for gas analysis (1) which was placed in the system as shown in Figure 2. The gas mixture was 7% CO_2 in air purchased from Scott Specialty Gases. The concentration of the mixture was verified by gas chromatography. The observed CO_2 and Oxygen (O_2) peaks were ratioed to the observed Nitrogen (N_2) peak. The dependence of the ratio upon the downstream pressure, P_2, at constant upstream pressure, P_1, for flow through the multichannel plate is shown in Figures 8 and 9. The resultant curves may be compared to data taken when the flange was not in the system and the gas was flowing through a piece of 6' long 1/8" diameter copper tubing. In the latter experiment, P_2 is the pressure at the gold leak, P_{GL}. The copper tubing data is shown in Figures 10 and 11. At equal applied pressure there is not a discernible difference between the multichannel plate and the tubing for the O_2/N_2 ratios in Figures 8 and 10. In the case of the CO_2/N_2 ratio differences do occur at low values of P_2. For example, at a P_2 of 2 torr and a P_1 of 12 torr the CO_2/N_2 ratio is .168 for the MCP while it is .16 for the copper tubing. The difference is experimentally real and is expected to become more significant at lower P_1.

In Figures 12 and 13 the mass flow for Ar, 15% CO_2 in air, Ne and He as a function of ΔP is presented for the empty flange and the multichannel plate, respectively. In both cases, the mass flow exhibits a linear dependence upon ΔP at constant P_1. Except for He the mass flow is considerably diminished for each gas, when the MCP is present.

FLOW MODELING

The nature of the flow through an opening can be separated into three regions of differing behavior. These three flow regions, viscous, transitional and molecular exist in different pressure ranges with overlap for the differing types of flow. Using the mean free path, defined as:

$$\lambda = \frac{16\ \mu}{5\ P_1} \sqrt{\frac{RT}{2\pi M}} \qquad (1)$$

rough limits for the existence of these three types of flow can be established (2). At a value of r/λ less than 1, where r is the radius of the capillary opening, molecular flow should dominate. For r/λ values between 1 and 100 the flow should be transitional and above 100 it is viscous. For the array of capillaries used in this experiment, with a radius of 4.9 μm, r/λ is always below 100 and becomes less than 1 at pressures below 10 torr. The above is simply a rough guide to establish a background for the more extensive flow treatment an analysis discussed below.

The measured mass flow can be compared with what might be expected for free molecular flow by determining the ratio $\dot{m}/\dot{m}_{fm}$, where $\dot{m}$ is the measured mass flow and $\dot{m}_{fm}$ is the calculated free molecular mass flow at the temperature and pressure of the measured mass flow. Free molecular is defined by the following expression:

$$\dot{m}_{em} = k\pi r^2 P_1 \left(1 - \frac{P_2}{P_1}\right) \sqrt{\frac{M}{2\pi RT}} \qquad (2)$$

where k is the Clausing constant determined from tables in reference 2. For the capillaries in this experiment the L/d was approximately 40 and

the corresponding value of k was .0613. The molecular weight, M, in equation 1, is an average molecular weight in the case of gas mixtures.

The nondimensionalized mass flow $\dot{m}/\dot{m}_{fm}$ as a function of the pressure ratio P_1/P_2 is shown in Figures 14 and 15 for the 15%-CO_2 air mixture and pure Argon, respectively. At low P_1 (less than 5 torr) the observed ratio is approximately 1 for the limited pressure ratio that was accessible in this experiment. At slightly higher 11.89 torr, in the case of the CO_2 air mixtures, the non-dimensional flow is observed to pass through a maximum as the pressure ratio is decreased. The maximum in the flow has also been observed by Sreekanth (3,4) for the case of flow through one capillary opening. Sreekanth's studies were for a lower external pressure than available in the current experiment. As the external pressure is raised the mass flow ratios converge at a limiting value indicating the onset of choked flow. It is possible to define a Knudsen number, K_n, for the current experimental situation as

$$K_n = \frac{\lambda}{d} \tag{3}$$

The range of Knudsen numbers is from approximately .8 to 2.5 which is precisely the range covered by Sreekanth's experiments.

To further characterize the flow through the multichannel plate, the discharge coefficient (the ratio of actual mass flow to one-dimensional isentropic mass flow for choked conditions) can be determined. The discharge coefficient is defined as:

$$C_D = \frac{\dot{m}_{meas}}{\dot{m}_{isen}} = \frac{\dot{m}_{meas}}{\left[\frac{\gamma}{R}\left(\frac{2}{\gamma+1}\right)^{\frac{\gamma+1}{\gamma-1}}\right]^{1/2} \frac{P_1 A}{T}} \qquad (4)$$

The dependence of the discharge coefficient upon the Reynolds number is shown in Figures 16 and 17. The Reynolds number is defined as:

$$Re = \frac{2\dot{m}}{\mu r \pi} \qquad (5)$$

As the applied pressure increases the values of the discharge coefficient begin to converge as choked flow is approached. At low Reynolds number the flow approaches that expected for free molecular flow.

Willis (5) has evaluated the mass flow through a circular orifice at high pressure ratios. He was able to derive an expression for the nondimensionalized mass flow using an expansion in Re. The resultant expression is:

$$\frac{\dot{m}}{\dot{m}_{fm}} = 1 + .083\ Re + 0\ (Re) \qquad (6)$$

This expression was found to fit a variety of existent experimental data at suitably low pressures. For the one experimental case in this report, where there is sufficient data, the observed value of the linear coefficient was .095, in reasonable agreement with that predicted in equation 6. However,

there is not, as of yet, sufficient data available for any firm conclusions about the multichannel plate.

There have been two previous studies of capillary arrays similar to the one described in this report (6,7). In both cases the primary objective was the production of molecular beams with an analysis of the shape of the beam and peak intensity. Giordmaine and Wang (6) were able to calculate the peak beam intensity and beam width assuming that their is limited Knudsen flow near the low pressure end of the capillary source. Johnson, Stein and Pritchard (7) were able to express the flow rate in terms of plate parameters and the nature of the gas. Their resultant expression is given below:

$$\frac{Q}{A} = \frac{2}{3}\left(\frac{\sqrt{2}}{3\pi}\right)\left(\frac{\bar{V}}{\sigma^2}\right)\left(\frac{L}{\lambda}\right)\left(\frac{\varepsilon}{\lambda}\right)\left(\frac{r}{\lambda}\right) \qquad (7)$$

The above expression will be utilized in studies conducted upon the apparatus described in the next section which will be able to achieve pressures where free molecular flow can exist in the multi-channel plate.

LABORATORY MODELING

The redesigned multichannel plate holder is shown in Figure 18 a,b. The holder is designed to allow for flow parallel to the surface of the MCP. The MCP is mounted on a teflon disk which is between the MCP and the various masks that will be used. The teflon disk provides a sealing surface to insure that the gas flow will occur through the MCP and not around the edges. In addition, the metal mask is held against an "O" ring seal to facilitate the achievement of a low external pressure as well as to further reduce the chance of leakage of the flow to the mass spectrometer. The

array of MCP, teflon disk and mask is firmly clamped in the holder. At this point in time we have been able to achieve a pressure reading of 10^{-3} torr with a mechanical pump on the external side of the MCP and a turbomolecular pump downstream of the MCP.

The experimental apparatus, with the MCP holder in place, is shown in the schematic in Figure 19. The pressure measurements, P_i and ΔP, will be made by either thermocouple gages or Barocel pressure transducers depending upon the pressure range of the particular experiment. The flowmeter is a Hastings mass flowmeter as before. The mass spectrometer is different from that used in previous experiments, a quadropole mass spectrometer purchased from Extranuclear Corp., their model C-50. The MS is capable of being placed under computer control. However the data described in this section was obtained by recording the signal on a strip chart recorder. The inlet to the MS was purchased from vacumetrics and contains a micrometer valve in addition to a bypass for efficient pumping of upstream lines. The entire system is pumped by a turbomolecular pump with the pressure monitored by an ionization gage.

The MCP used in these experiments has been coated with a metallic coating. As a result the average diameter of the holes has been reduced to 5.7 μm. This MCP is, then, only approximately 30% open space. For example, when the MCP is used with the mask with the 1/8" diameter hole there are approximately 2.7×10^3 holes in the MCP through which gas could flow. The thickness of the new plate is 400 μm, as before.

In the initial experiments, the admission of gas to the MS was controlled by the micrometer valve. As a result the flow through the lines downstream of the MCP was effectively throttled. The pressure drops across the MCP are not the pressure drops that might be obtained in a vigorously

pumped system. The data obtained with this configuration is presented in Table I-III for the three masks used. At this point in time, the only firm statement that can be made is that at pressures below 5 torr mass separation will begin to occur, as observed previously. Any firmer conclusions of greater generality will have to await further experimentation.

REENTRY MODELING

The gas chemistry that is occurring at the shock or at the surface of a proposed test vehicle (either satellite or reentry) can be modeled utilizing a program developed by Shinn et al. (8). The expected reaction products can be estimated assuming certain initial freestream conditions and the extent of surface catalysis. The information thus obtained will provide guidelines for the eventual construction of an onboard mass spectrometer with an inlet system.

In this section the results of a calculation for a particular reentry vehicle are presented and discussed. The calculations were performed by D. Eide (9). The assumed vehicle shape is a combination of a 55° cone with a spherical blunt nose. The angle of attack is 35°. The physical conditions and the concentrations of O, N, NO, N_2, and O_2 are calculated from the surface to the shock boundary, assuming the free stream conditions given in Table IV at the four altitudes under consideration: 84 km, 73 km, 65 km, and 55 km. The calculations were performed at various stations along the vehicle centerline. All results presented in this report are at stations which are downstream of the point at which the geometry of the sphere is mathematically merged with the cone to generate the shape of the vehicle. The nondimensional coordinates of the various stations selected are shown in

Table V. These coordinates are defined in reference 8. The reentry path of the vehicle is that for a typical shuttle reentry.

The dependence of some of the important physical parameters, pressure, temperature, density and viscosity, upon altitude and distance from the vehicle surface are shown in Figures 20-30. All of the parameter values are normalized by their value at the boundary layer. The distance from the surface is normalized by the boundary layer thickness. The values for the boundary layer thickness and the parameters at the boundary layer edge are shown in Table VI. The largest variation in the nondimensional physical parameters with altitude is at station 12, the closest site to the stagnation point. Further downstream on the centerline there is little variation as the vehicle traverses a flight path from 84 km to 55 km.

The temperature varies more slowly across the boundary layer than any of the other physical parameters. At the two lowest altitudes, at station 12 shown in Figure 20, the boundary layer edge value is attained at a Y/Y_{b1} of approximately .5. At the two higher altitudes the boundary layer edge value is not attained until $Y/Y_{b1} = .9$. For the two other stations considered, shown in Figures 21 and 22, the variation is across the entire boundary layer and at the same spatial rate at all altitudes.

The density decreases across the boundary layer rather than increasing as does the temperature. The decrease to the boundary layer edge value is accomplished at a $Y/Y_{b1} = .4$ at all altitudes at station 12, as shown in Figure 23. At station 12 the density at the wall is less than that at the boundary layer edge at an altitude of 84 km. At the other stations the density is always greater than the boundary layer edge value at all altitudes as shown in Figures 24 and 25.

The increase in viscosity is almost as slow as that of the temperature and as shown in Figures 26-28. As in the case with the temperature, the viscosity tends to attain the same spatial rate at all altitudes at test stations that are further downstream from the stagnation point.

The pressure remains relatively constant within the boundary layer at all altitudes, as shown in Figures 29 and 30. The variation in pressure is also fairly small along the surface of the vehicle. The highest pressure that will be attained, for this flight path, is approximately 7×10^2 atm (53 torr) at 55 km.

The chemical composition within the boundary layer, at the four chosen altitudes, is shown in Figures 31-45. The mole fractions are normalized by their values at the boundary layer edge as were the physical parameters. The values for the mole fraction and the number density, at the boundary layer edge, of each species considered in the calculation, O, O_2, N, N_2, and NO are shown in Table VII-X. At the altitudes considered in this report the predominant molecular species is N_2 followed by O atom and N atom. Several of the species reach values within the boundary layer which are higher than their values at the boundary layer. Molecular oxygen is always higher than or equal to its boundary layer value. Again the greatest variation in composition with altitude occurs at station 12, the site nearest the stagnation point.

REFERENCES

1. Wood, G.M. and Yeager, P.R. Environmental and Climatic Impact of Coal Utilization, J.J. Singh and A. Deepak, eds. Academic Press, NY (1980) 187.

2. Dushman, S., Scientific Foundations of Vacuum Technique, 2nd ed. (J. M. Lafferty, ed.) Wiley, New York (1962).

3. Sreekanth, A.K., Boeing Scientific Research Laboratories, TN 86 (1963).

4. Sreekanth, A.K., Boeing Scientific Research Laboratories, Report No. D1-82-0427, April 1965.

5. Willis, D.R., J. Fluid Mech., 21, 21 (1965).

6. Giordmaine, J.A. and Wang, T.C., J. Appl. Phys. 31, 463 (1960).

7. Johnson, J.C., Stair, A.T. and Pritchard, J.L., J. Appl. Phys. 37, 1551 (1966).

8. Shinn, J.L., Moss, J.N. and Simmonds, A.L., AIAA Paper No. 82-0842 June 1982.

9. Eide, D., personal communication.

TABLES

Table I. Flow of 7.55% CO_2 in Air through the Coated MCP with a mask with a 1/8" diameter hole.

P_1 (torr)	flow (sccm)	ΔP (torr)	$\frac{I(CO_2)}{(IN_2)}$	$\frac{I(O_2)}{I(N_2)}$	$\frac{I(CO_2)}{I(O_2)}$
0.10	0.3	0.00	0.13	0.193	0.68
0.17	0.3	0.01002	0.14	0.198	0.70
0.18	0.77	0.02003	0.14	0.198	0.70_5
1.15	0.3	0.00	0.14	0.201	0.72
1.10	0.70	0.01	0.140	0.192	0.732
1.17	3.5	0.05	0.14	0.196	0.73
1.54	7.06	0.10	0.147	0.203	0.723
5.16	0.3	0.00	0.15	0.200	0.76
5.15	0.70	0.00	0.15	0.198	0.76
5.09	3.5	0.01	0.15	0.200	0.75
5.17	7.00	0.03	0.15	0.199	0.76
9.96	0.3	0.00	0.155	0.201_5	0.769
9.97	0.70	0.00	0.15	0.201_5	0.76
9.88	3.6	0.01	0.15	0.201	0.76_5
10.04	7.06	0.01	0.15_5	0.202	0.77

Table II. Flow of 7.55% CO_2 in Air through the coated MCP with the mask with a 1/16" diameter hole.

P_1 (torr)	flow (sccm)	ΔP (torr)	$\frac{I(CO_2)}{(IN_2)}$	$\frac{I(O_2)}{I(N_2)}$	$\frac{I(CO_2)}{I(O_2)}$
<0.10	0.3	0.02	0.12	0.187	0.66
0.17	0.3	0.01	0.13	0.196	0.67
0.18	0.70	0.02	0.13_5	0.197	0.69
1.11	0.3	0.01	0.14_5	0.201	0.72
1.05	0.70	0.01	0.15	0.201	0.73
1.12	3.0	0.06	0.15	0.201	0.73
1.51	7.06	0.10	0.147	0.204	0.719
4.91	0.3	0.00	0.15	0.203	0.76
5.04	0.70	0.01	0.15_5	0.203	0.76
5.01	3.6	0.02	0.15_5	0.202	0.77
5.09	7.06	0.04	0.16	0.203	0.77
9.97	0.3	0.00	0.16	0.205	0.77
9.79	0.70	0.01	0.16	0.205	0.76
9.84	3.6	0.01	0.16	0.204	0.78
9.91	7.00	0.02	0.16	0.205	0.78

Table III. Flow of 7.55% CO_2 in Air through the coated MCP with the mask with a 1/32" diameter hole.

P_1 (torr)	flow (sccm)	ΔP (torr)	$\frac{I(CO_2)}{(IN_2)}$	$\frac{I(O_2)}{I(N_2)}$	$\frac{I(CO_2)}{I(O_2)}$
<0.10	0.3	0.02003	0.132	0.196_5	0.673
0.17	0.3	0.01	0.14	0.196	0.70
0.18	0.70	0.03	0.14	0.198	0.70
1.04	0.3	0.01	0.14	0.197	0.73
1.04	0.70	0.02	0.14	0.198	0.72
1.08	3.5	0.06	0.14	0.198	0.73
1.53	7.00	0.10	0.15	0.203	0.729
4.95	0.3	0.01	0.15	0.202_5	0.75
5.00	0.70	0.00	0.15	0.202_5	0.75
5.08	3.5	0.02	0.15	0.203	0.76
5.09	7.06	0.03	0.15	0.203	0.75_5
9.88	0.3	0.01	0.16	0.204	0.77
9.88	0.70	0.01	0.16	0.205	0.77_5
9.86	3.6	0.01	0.16	0.203	0.78
9.88	7.13	0.02	0.16	0.203	0.77

Table IV. Free Stream Parameters.

Alt(km)	T(K)	P(atm)	M(amu)	V(Km/s)
84	190	5.24×10^{-6}	28	7.75
73	213	3.24×10^{-5}	22	6.98
65	233	1.08×10^{-4}	18	5.51
55	265	4.13×10^{-4}	13	4.24

Table V. Non-dimensional Shuttle Coordinates* of the Test Stations.

Station	X	Y
12	.013	.017
24	.069	.030
30	.159	.052

*Described in reference 8.

Table VI. Physical Parameters at the Boundary Layer Edge.

Alt(km)	Station	Y_{BL}(m)	T(K)/10^4	P(atm)/10^{-2}	P(kg/m^3)/10^{-4}	$\mu(\frac{N-s}{m^2})/10^{-3}$
84	12	.069	1.25	.39	.968	.239
84	24	.043	.81	.40	1.28	.193
84	30	.064	.73	.40	1.36	.182
73	12	.018	.83	1.49	5.1	1.87
73	24	.019	.63	1.53	6.8	1.54
65	12	.019	.67	3.35	14.6	.157
65	24	.012	.53	3.45	18.8	.133
65	30	.015	.48	3.44	20.6	.125
55	12	.019	.49	6.79	44.7	.122
55	24	.008	.40	6.97	54.2	.107
55	30	.009	.36	6.96	59.3	.101

Table VII. Number Density and Mole Fraction of Atomic and Molecular Species at the Boundary Layer Edge at an Altitude of 84 km.

Station	Species	$PN/10^{15}$	X_n
12	O	.462	.19
	O_2	.184	.076
	N	.146	.06
	N_2	1.54	.64
	NO	.087	.036
24	O	1.11	.29
	O_2	.005	.0014
	N	.852	.22
	N_2	1.73	.456
	NO	.10	.026
30	O	1.24	.29
	O_2	.002	3.7×10^{-4}
	N	1.16	.28
	N_2	1.76	.42
	NO	.048	.01

Table VIII. Number Density and Mole Fraction of Atomic and Molecular Species at the Boundary Layer Edge at an Altitude of 73 km.

Station	Species	$PN/10^{15}$	X_n
12	O	3.81	.276
	O_2	.105	7.65×10^{-3}
	N	1.37	.1
	N_2	7.67	.557
	NO	.81	.06
24	O	5.98	.32
	O_2	.03	1.72×10^{-3}
	N	1.67	.09
	N_2	10.7	.57
	NO	.45	.02

Table IX. Number Density and Mole Fraction of Atomic and Molecular Species at the Boundary Layer Edge at an Altitude of 65 km.

Station	Species	$PN/10^{15}$	X_n
12	O	10.8	.28
	O_2	.29	7.5×10^{-3}
	N	1.89	.05
	N_2	23.2	.6
	NO	2.29	.06
24	O	15.7	.32
	O_2	.28	5.64×10^{-3}
	N	1.14	.02
	N_2	31.1	.62
	NO	1.69	.03
30	O	1.24	.29
	O_2	.002	3.7×10^{-4}
	N	1.16	.28
	N_2	1.76	.42
	NO	.048	.01

Table X. Number Density and Mole Fraction of Atomic and Molecular Species at the Boundary Layer Edge at an Altitude of 55 km.

Station	Species	$PN/10^{15}$	X_n
12	O	17.7	.165
	O_2	8.4	.08
	N	.221	2.06×10^{-3}
	N_2	73.3	.684
	NO	7.58	.07
24	O	31.6	.23
	O_2	6.00	.04
	N	.13	9.7×10^{-4}
	N_2	90.1	.67
	NO	7.35	.05
30	O	34.8	.23
	O_2	7.53	.05
	N	.07	4.58×10^{-4}
	N_2	99.00	.67
	NO	6.7	.04

FIGURES

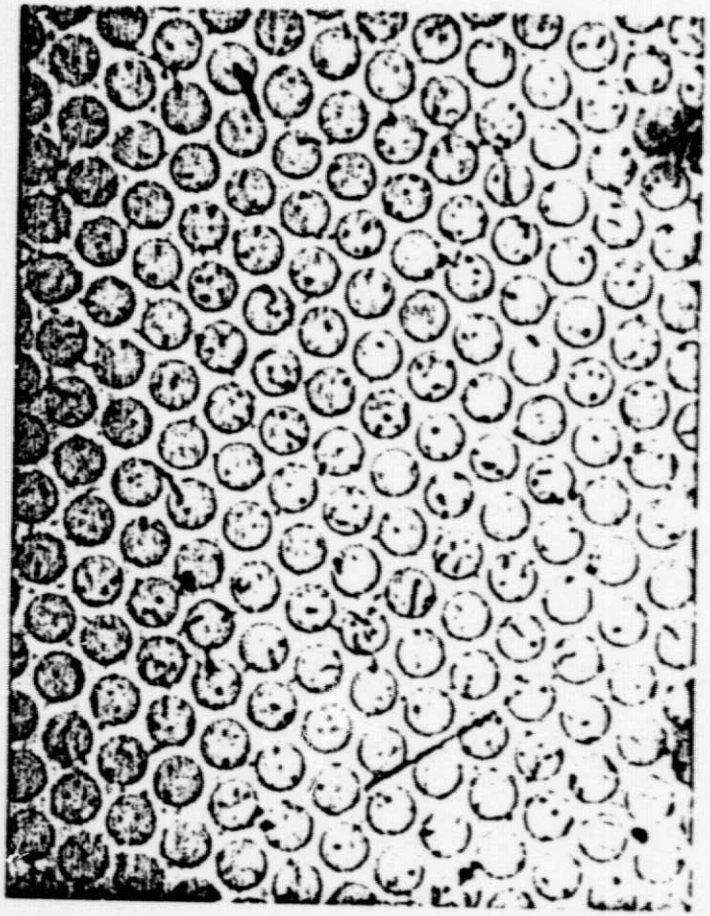

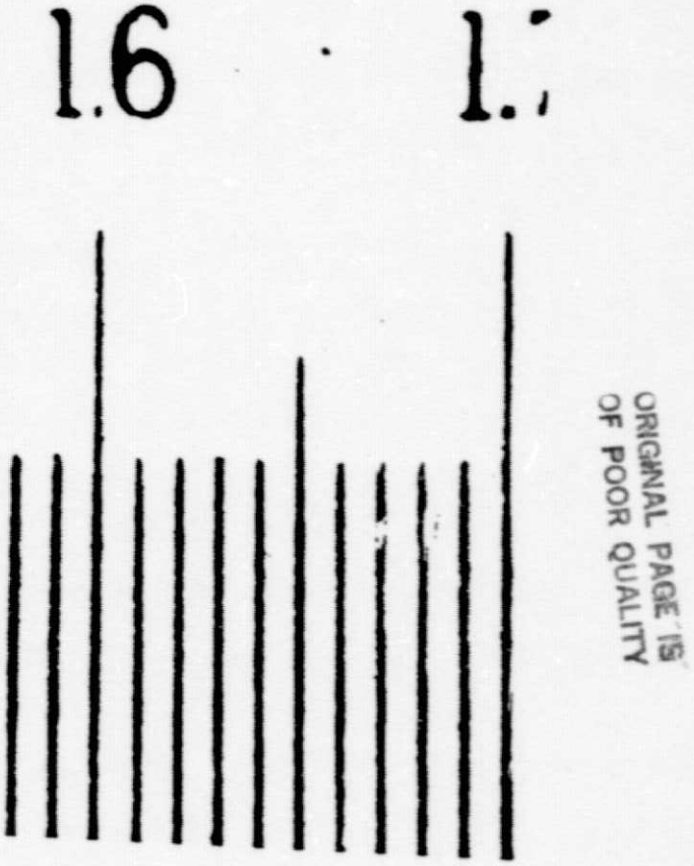

Figure 1. The multichannel plate at $5x10^3$ X magnification. The small divisions on the right represent 10μm.

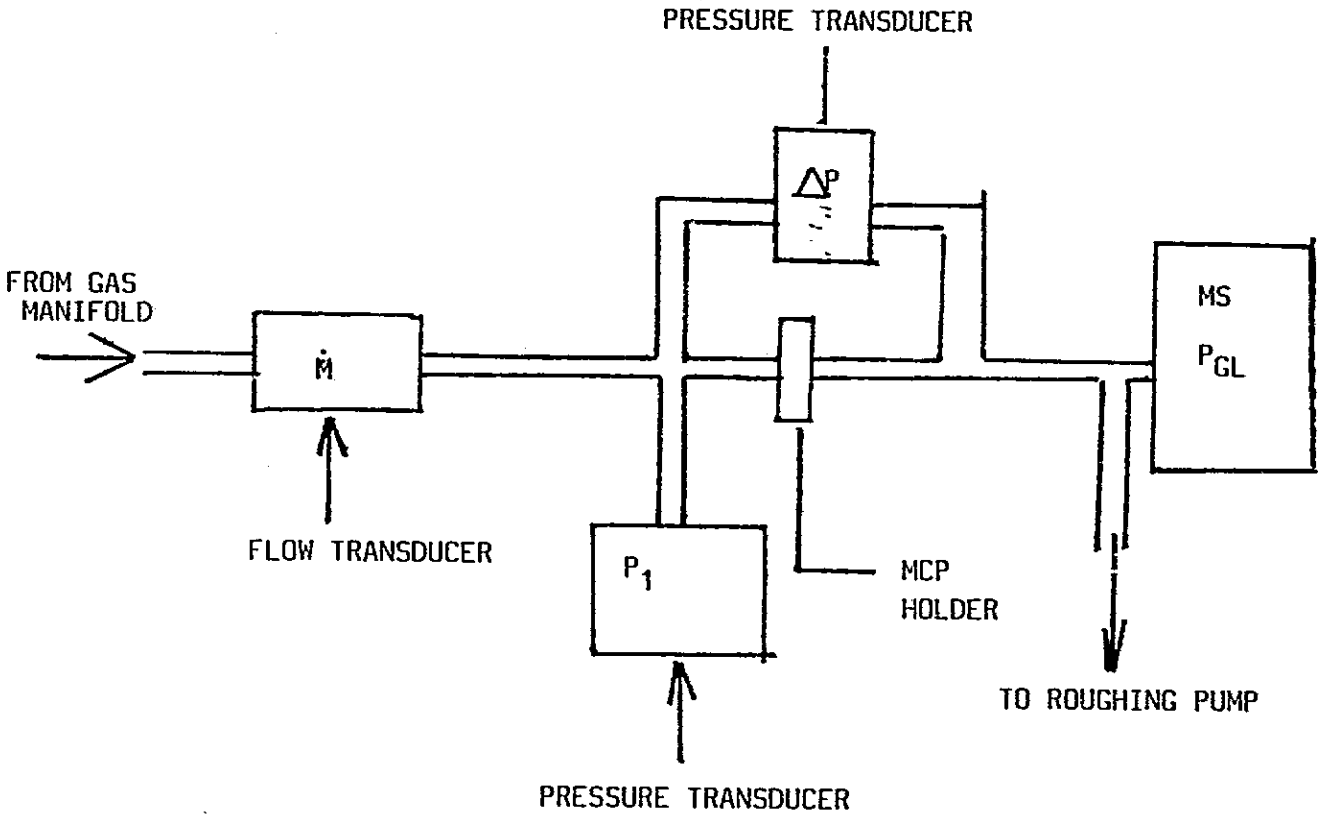

Figure 2. Initial experimental apparatus with the flow normal to the MCP. The mass spectrometer is a gas analysis and detection system developed at NASA-Langley (1).

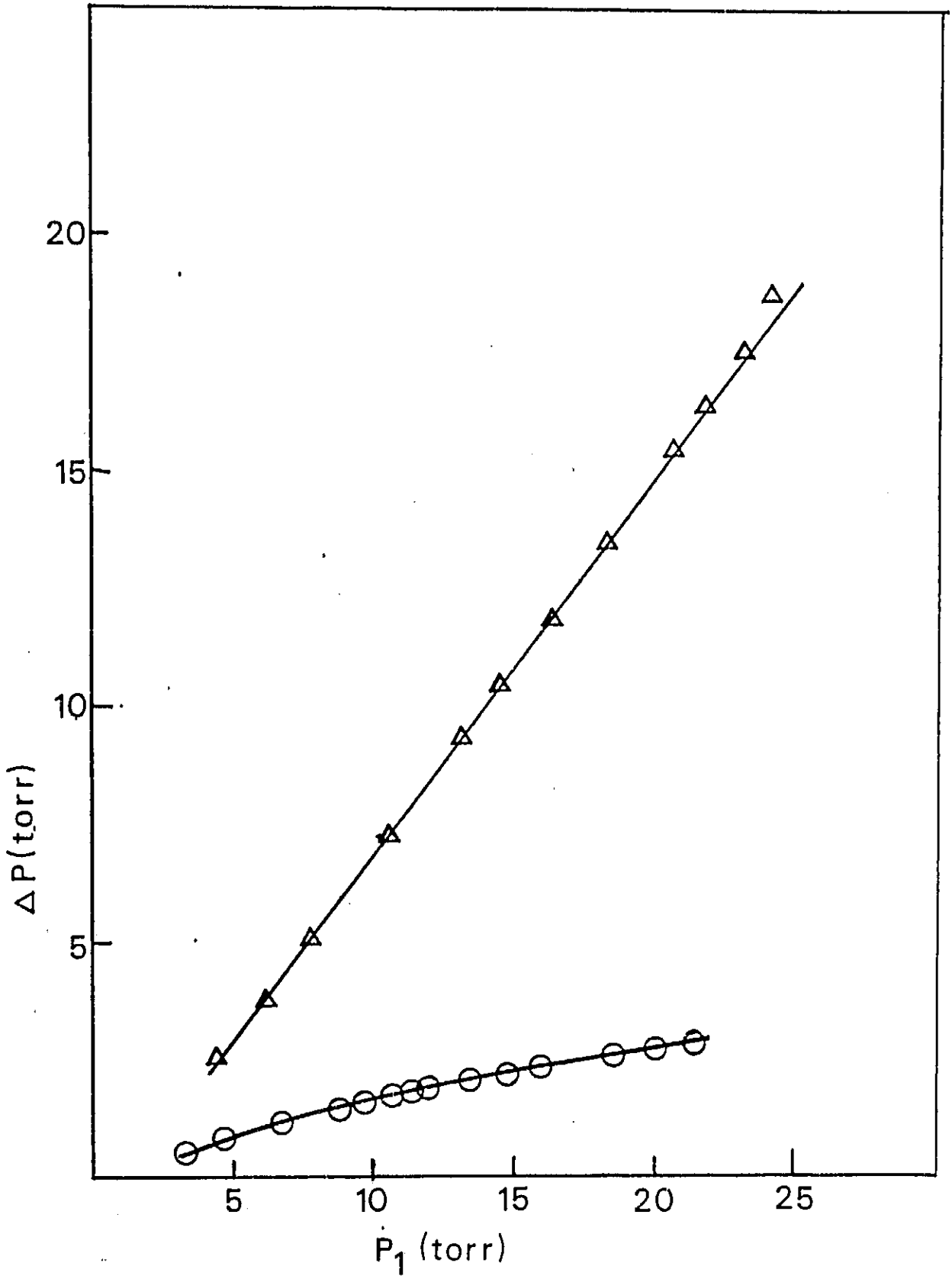

Figure 3. The pressure drop across the multichannel plate, ΔP, as the applied pressure P_1 is varied. Δ with effusive inlet. O without effusive inlet.

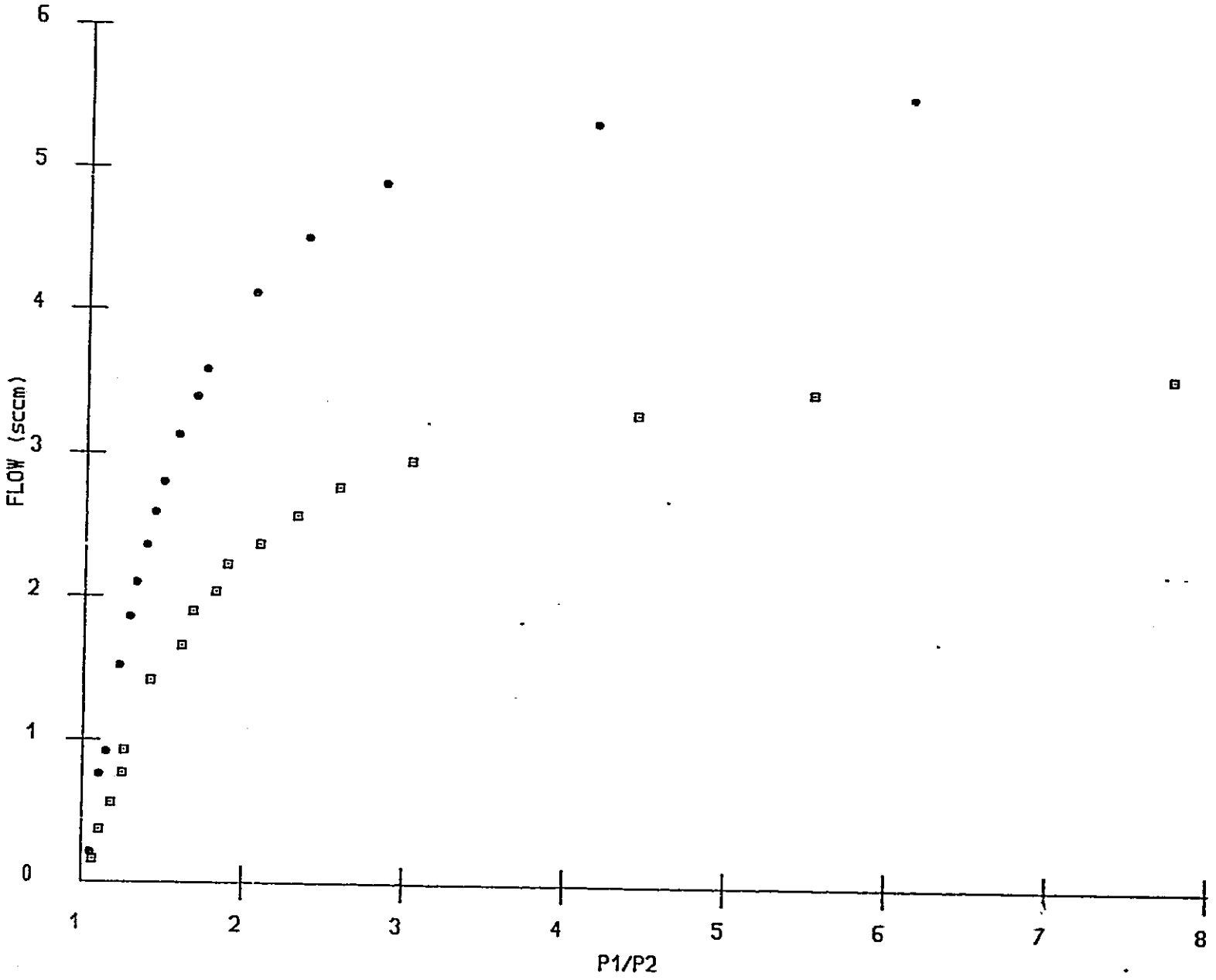

Figure 4. The dependence of the mass flow of Argon upon the ratio of the pressure, P_1, upstream of the flange to that of the pressure, P_2, downstream of the flange. O empty flange. ☐ multichannel plate in the flange. P_1 = 4 torr.

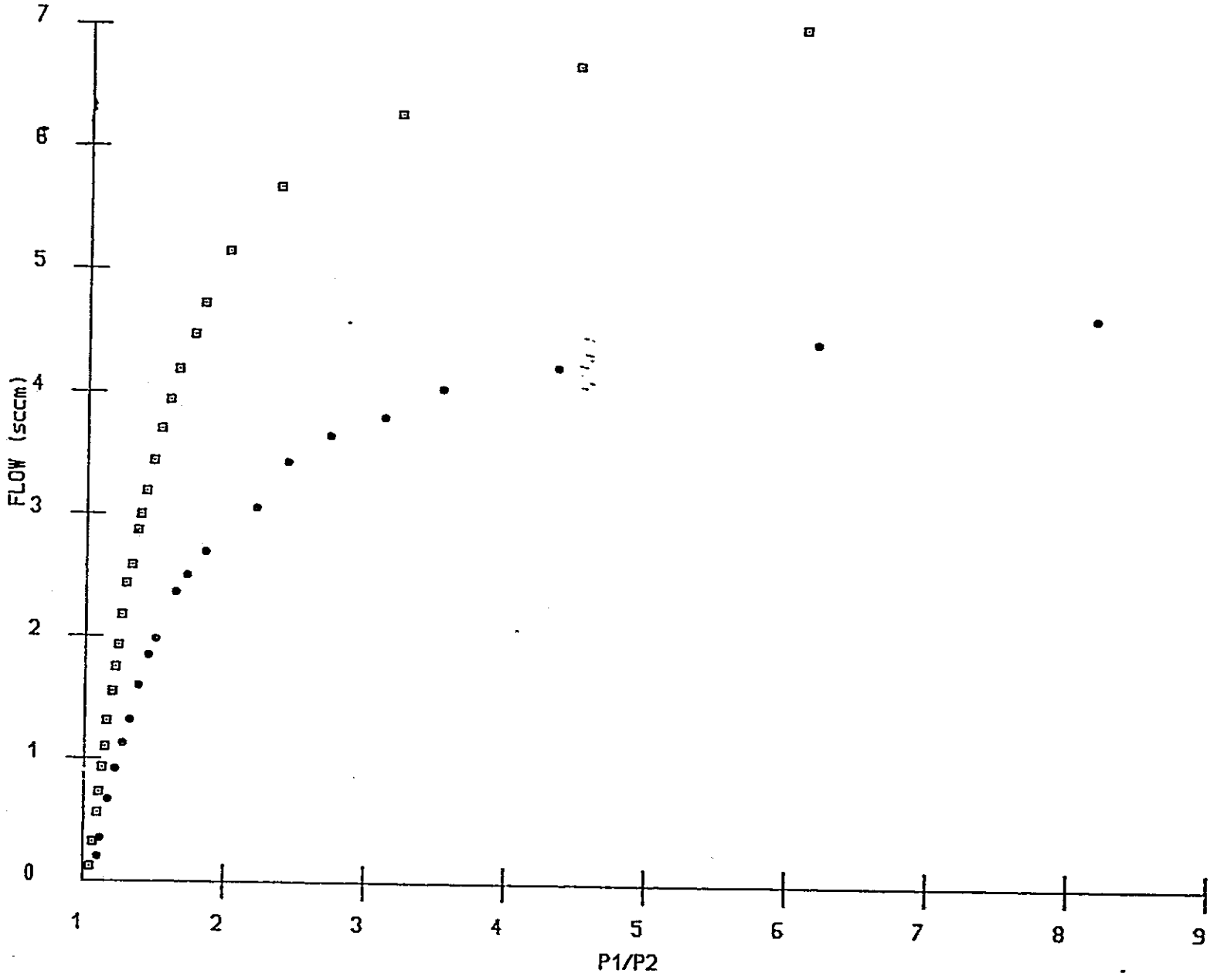

Figure 5. The same as figure 4 except that the gas is 15% CO_2 in air. □ empty flange, ○ MCP.

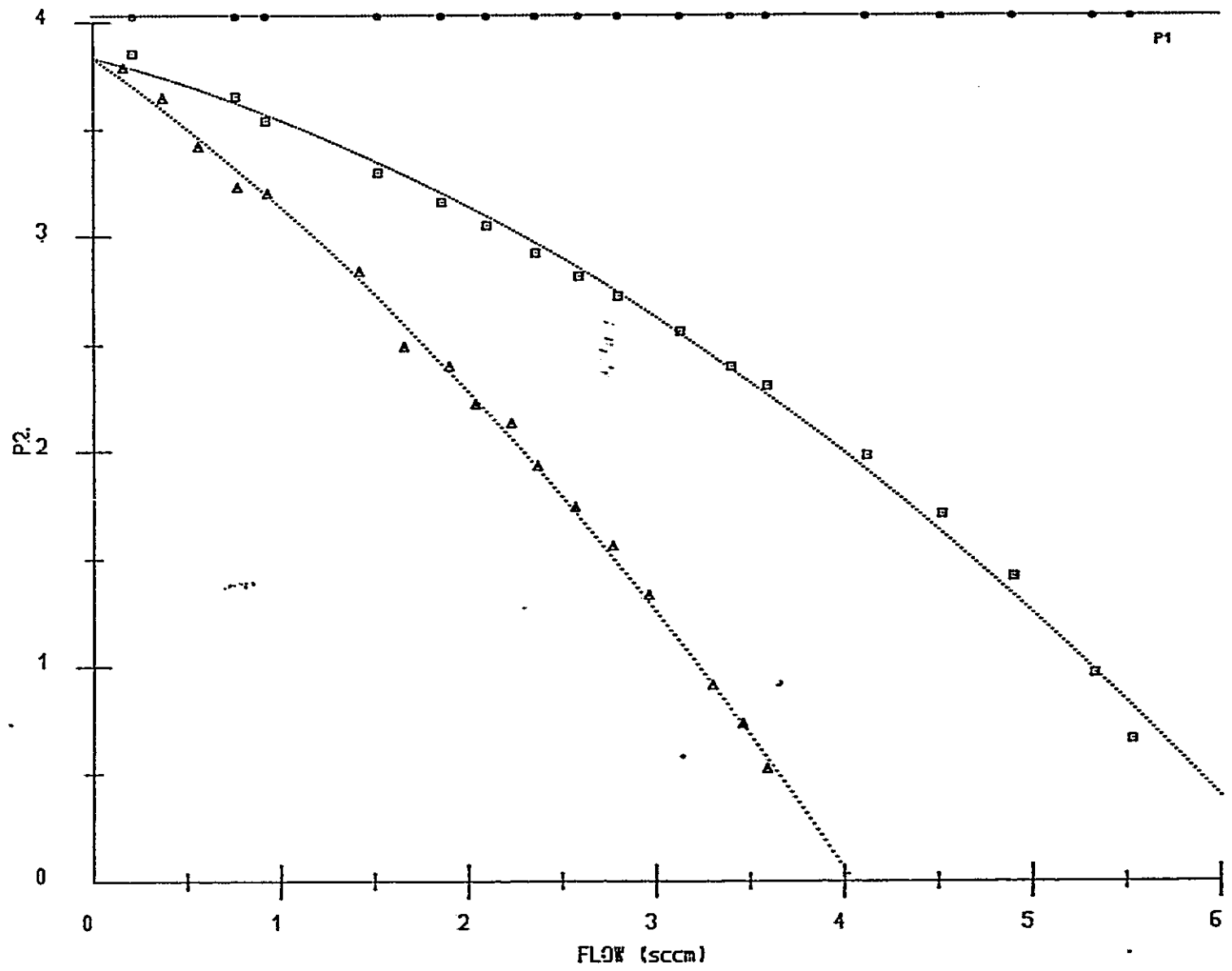

Figure 6. The downstream pressure, P_2, as the flow of the Argon is varied. □ empty flange. Δ MCP in flange. P_1 = 4 torr.

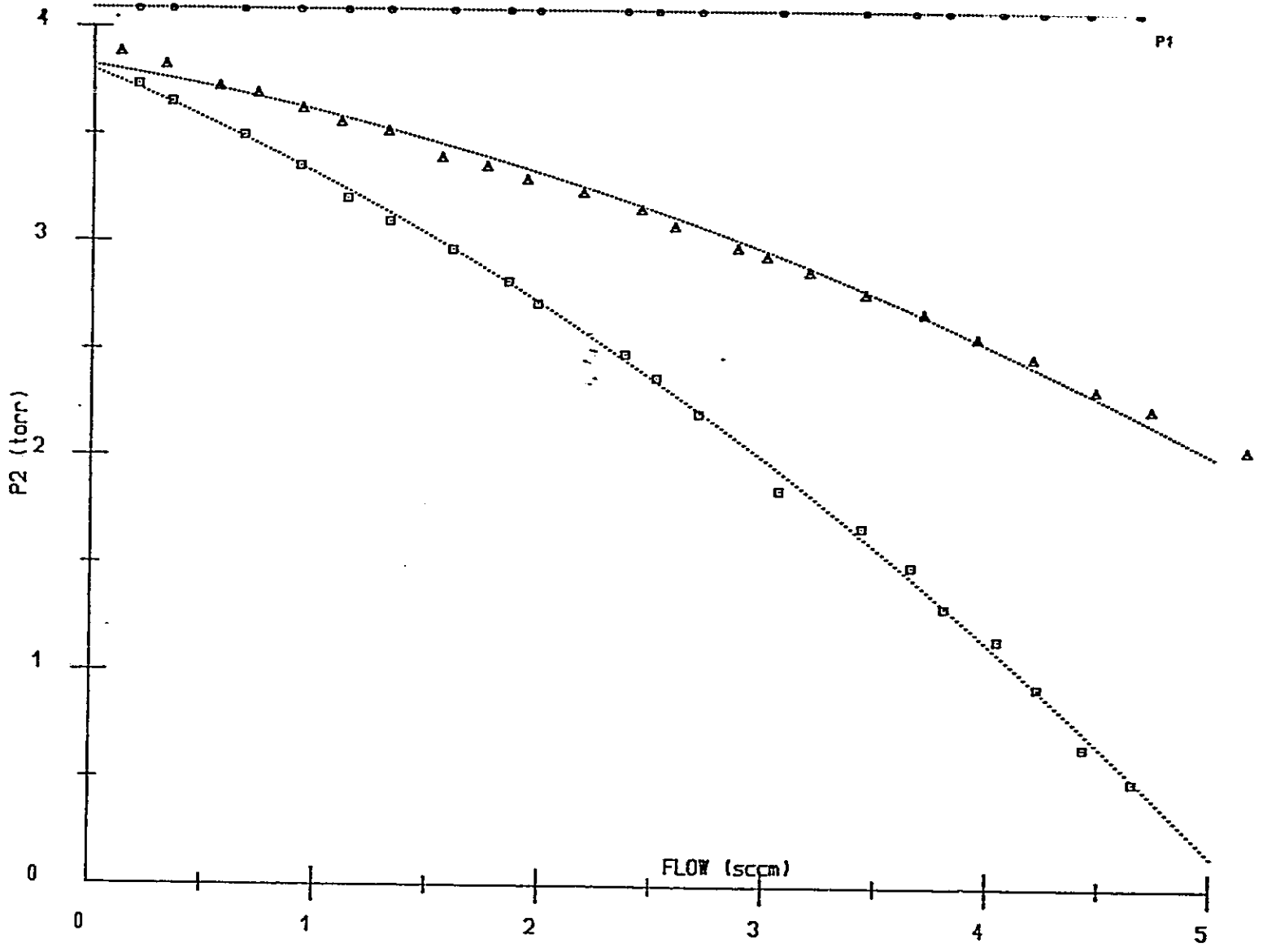

Figure 7. The same as figure 6 except the gas is 15% CO_2 in air. Δ empty flange, □ MCP.

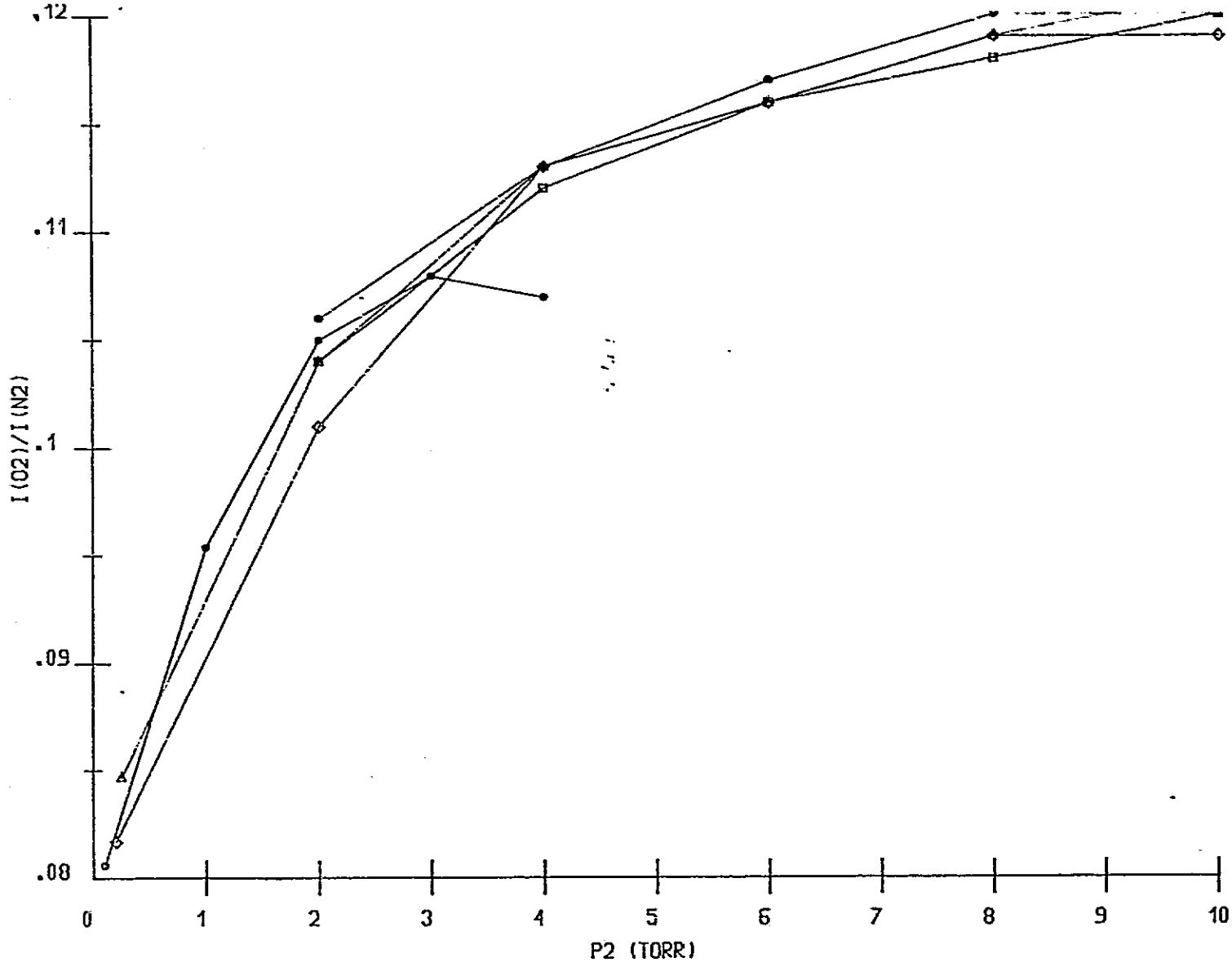

Figure 8. The ratio of the intensity of the O_2 peak at mass 32 to the intensity of the N_2 peak at mass 28 as the downstream pressure is varied at constant upstream pressures. The gas is 7% CO_2 in air and the direction of flow is normal to the MCP. P_1 = • 24 torr, □ 20 torr, Δ 15 torr, ◇ 12 torr, O 4.5 torr.

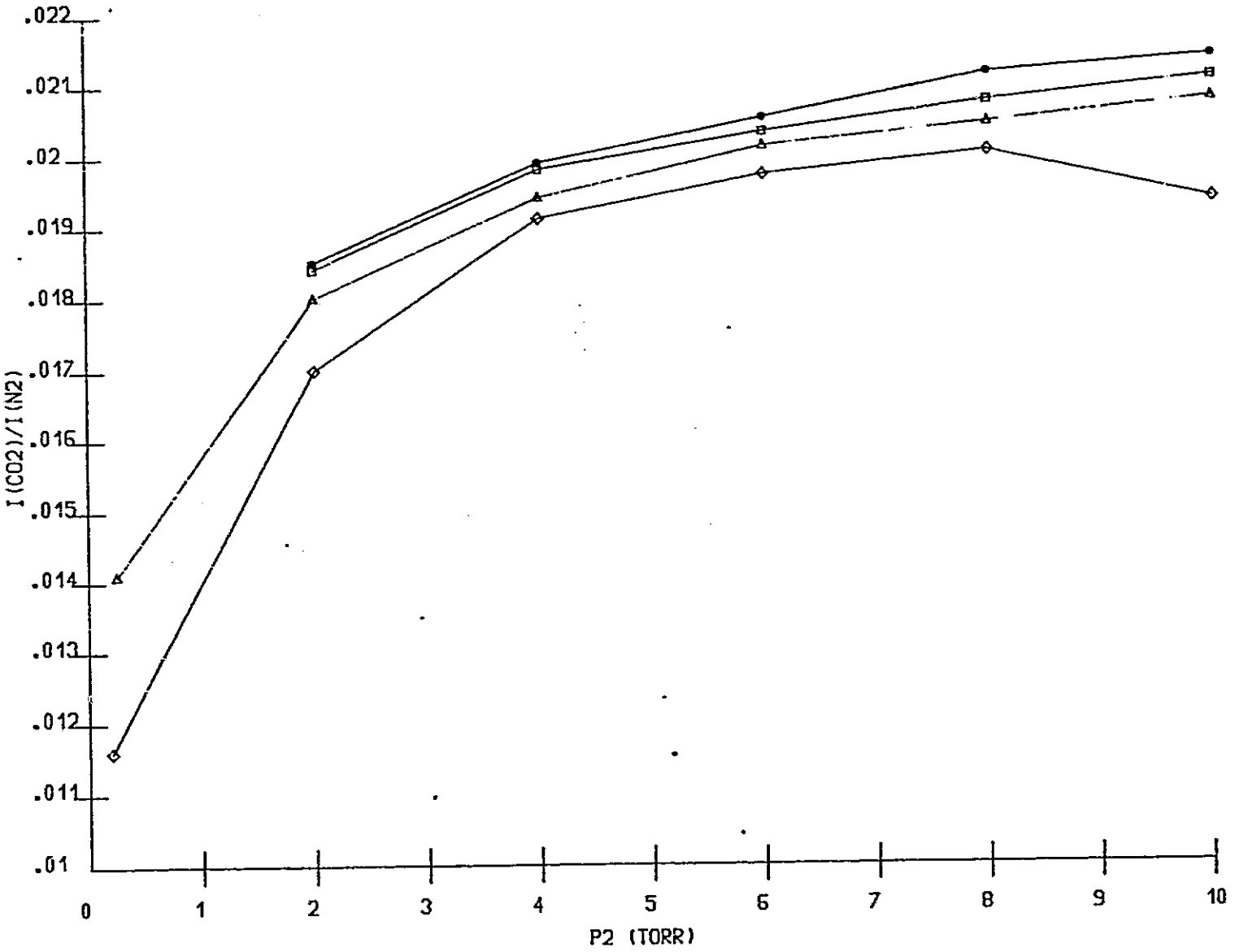

Figure 9. The ratio of the intensity of the CO_2 peak at mass 44 to the intensity of the N_2 peak at mass 28 as the downstream pressure is varied at constant upstream pressures. The gas is 7% CO_2 in air and P_1 = ⊗ 24 torr, □ 20 torr, Δ 15 torr, ◇ 12 torr.

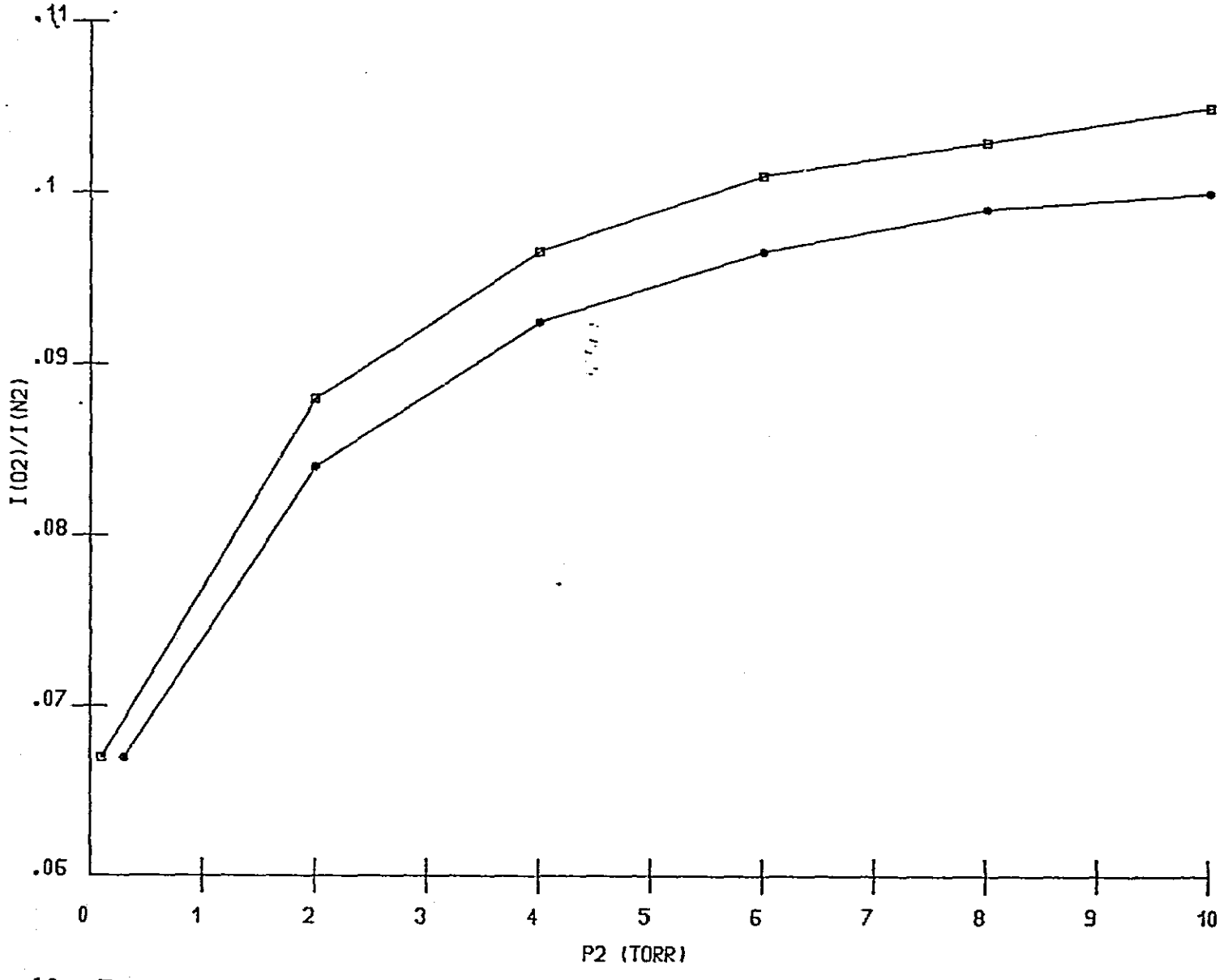

Figure 10. The ratio of the intensity of the O_2 peak at mass 32 to the intensity of the N_2 peak at mass 28 for a 7% CO_2 in air mixture flowing through 6 ft. of tubing. The downstream pressure, P_1, is the pressure at the mass spectrometer inlet. P_1 = □ 12 torr, 0 26 torr.

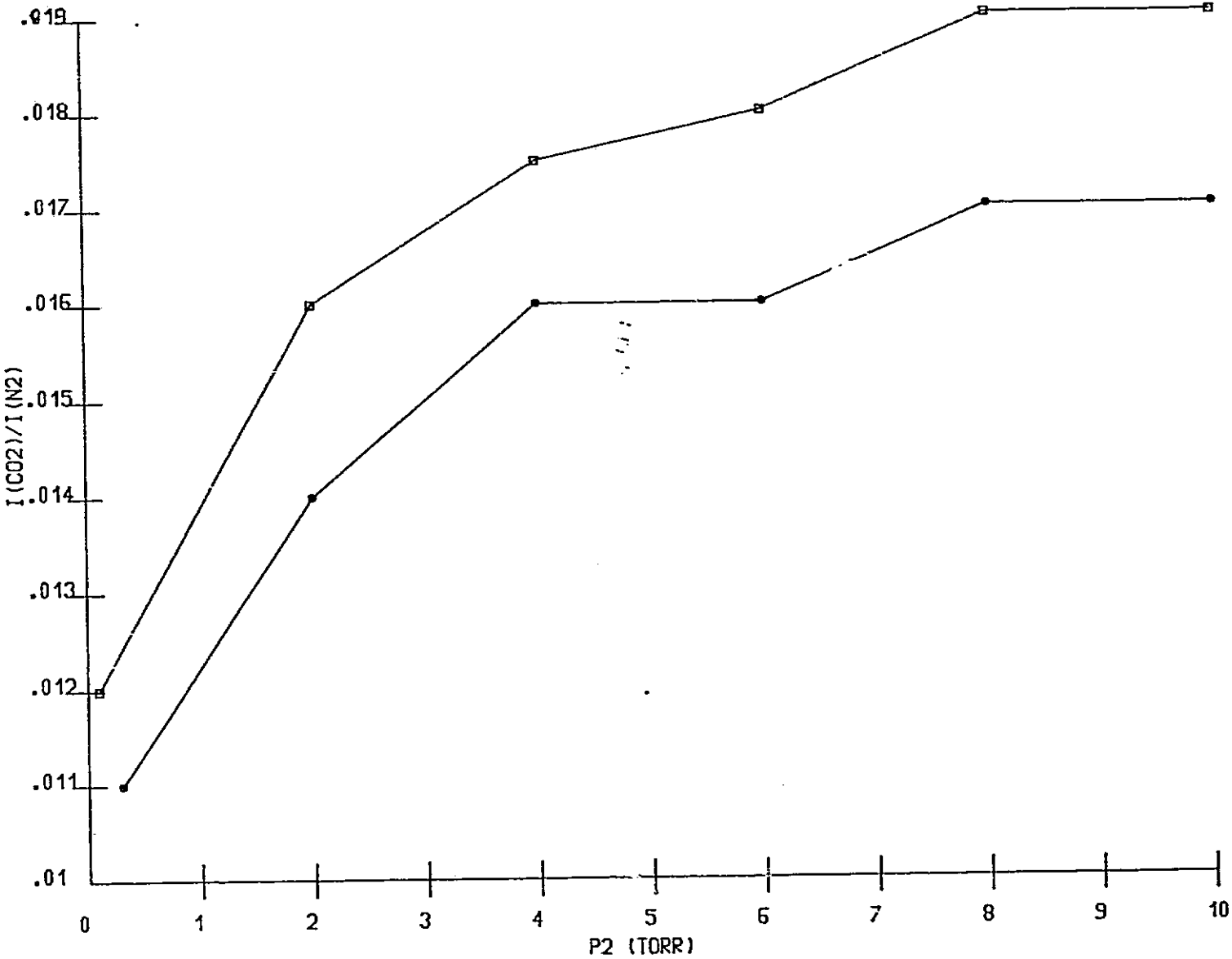

Figure 11. Same as figure 10 except that the intensity of the CO_2 peak at mass 44 is ratioed to the intensity of the N peak at mass 28. P_1 = □ 12 torr, 0 26 torr.

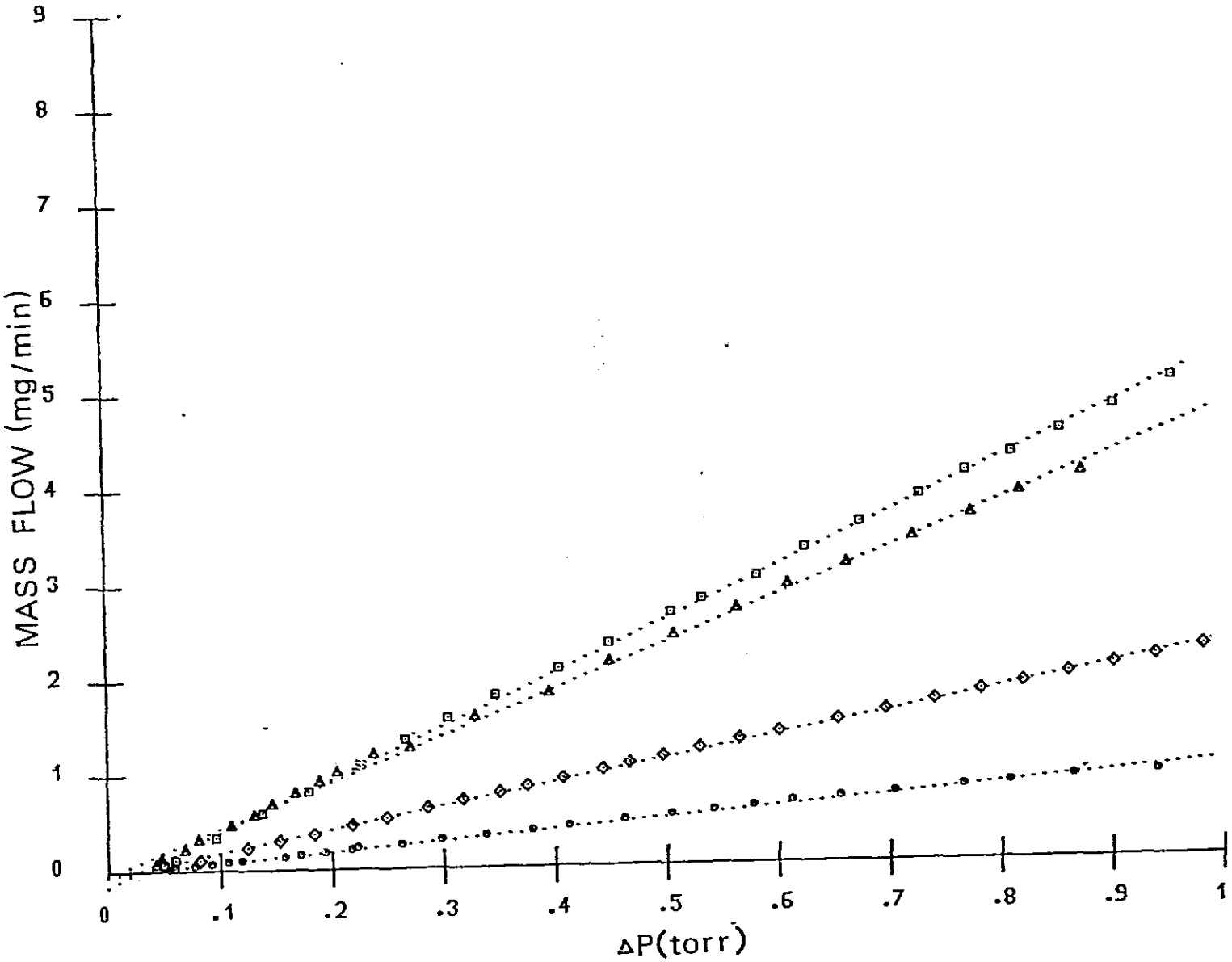

Figure 12. Mass flow for three pure gases and one gas mixture as a function of the pressure drop across the multi-channel plate. The upstream pressure is 1.72 torr except for the 15% CO_2 in air mixture where P_1 = 1.54 torr. □ Ar, Δ CO_2, ◇ Ne, ○ He.

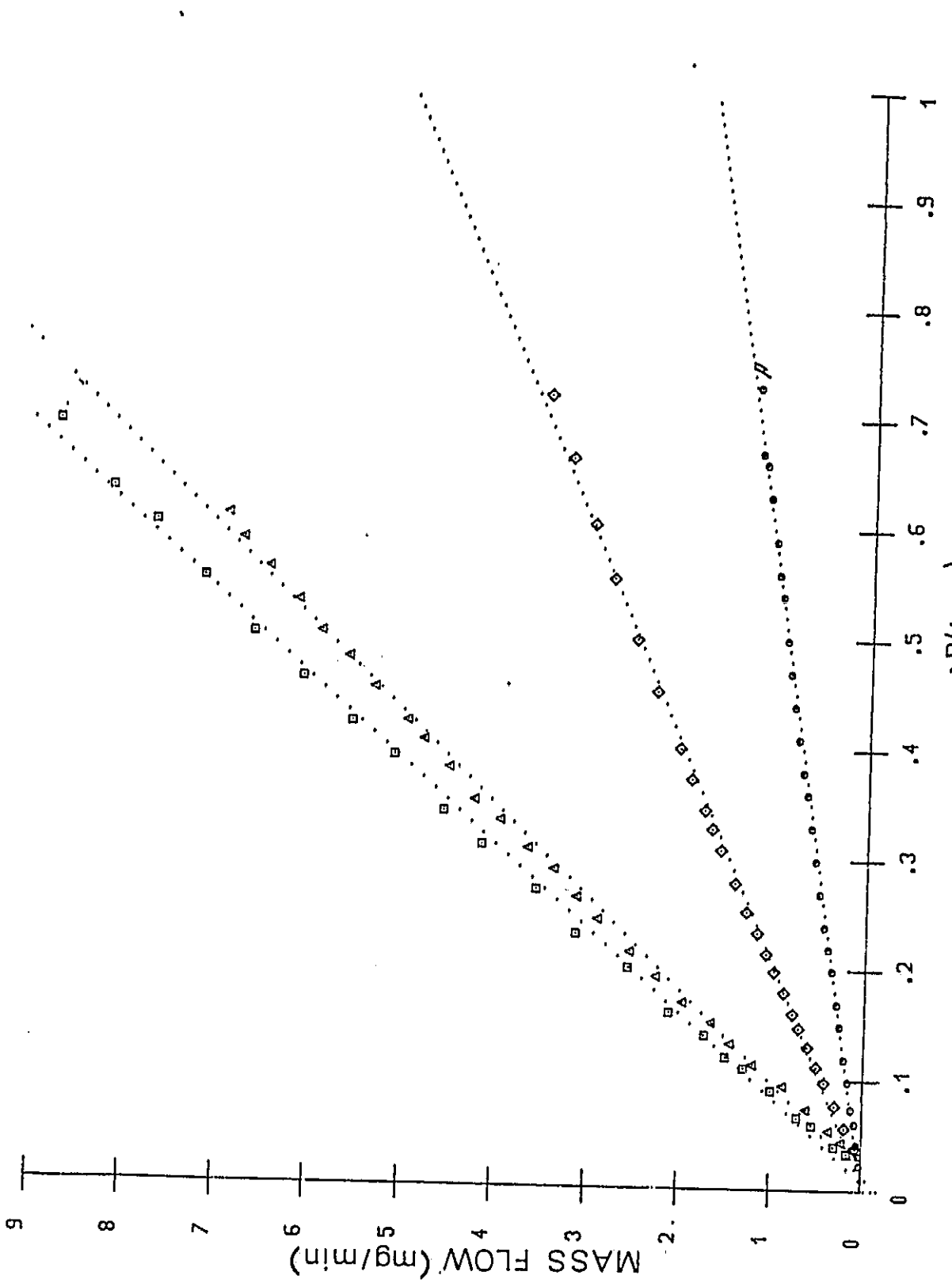

Figure 13. Same as figure 12 except that the multichannel plate is not in the flange.

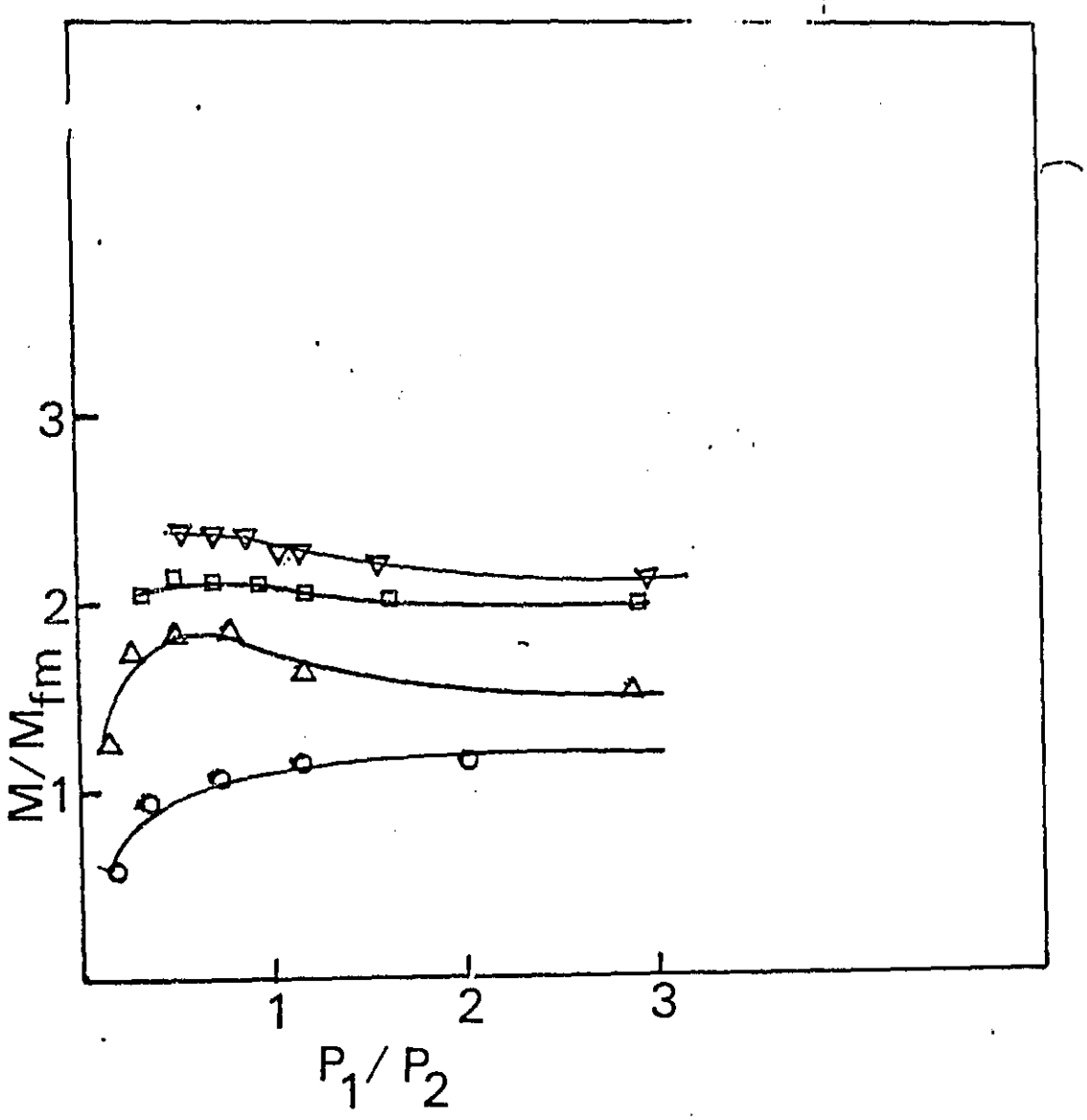

Figure 14. The non-dimensional mass flow through the multichannel plate as the ratio of the upstream pressure to the downstream pressure is varied at four values of the upstream pressure for the 15% CO_2 - air mixture. O P_1 = 4.39 torr, Δ P_1 = 11.89 torr, □ P_1 = 15.6 torr, ∇ P_1 = 20.4 torr.

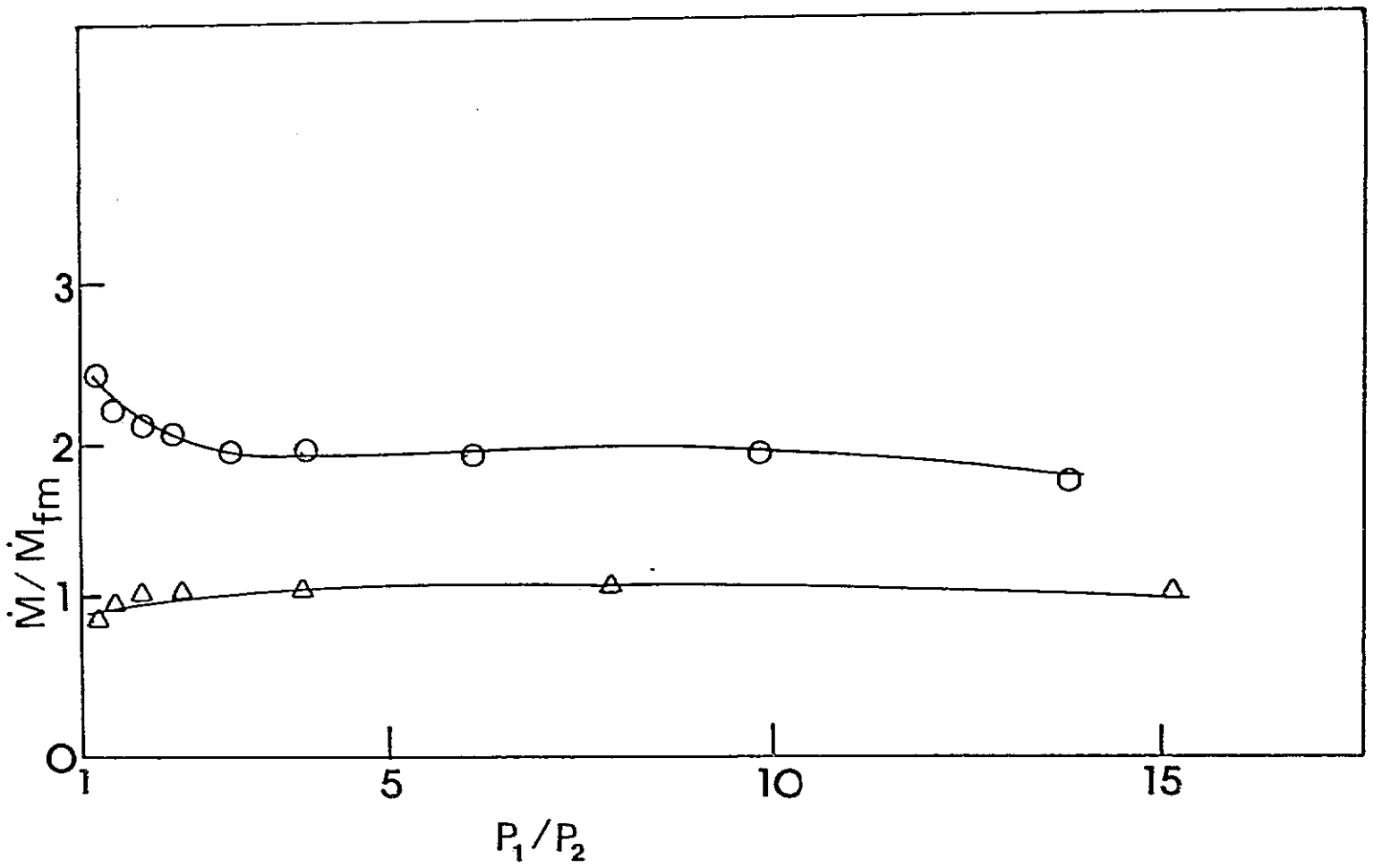

Figure 15. The non-dimensional mass flow of Argon through the MCP as the pressure ratio is varied. O P_1 = 8.33 torr, Δ P_1 = 5.8 torr.

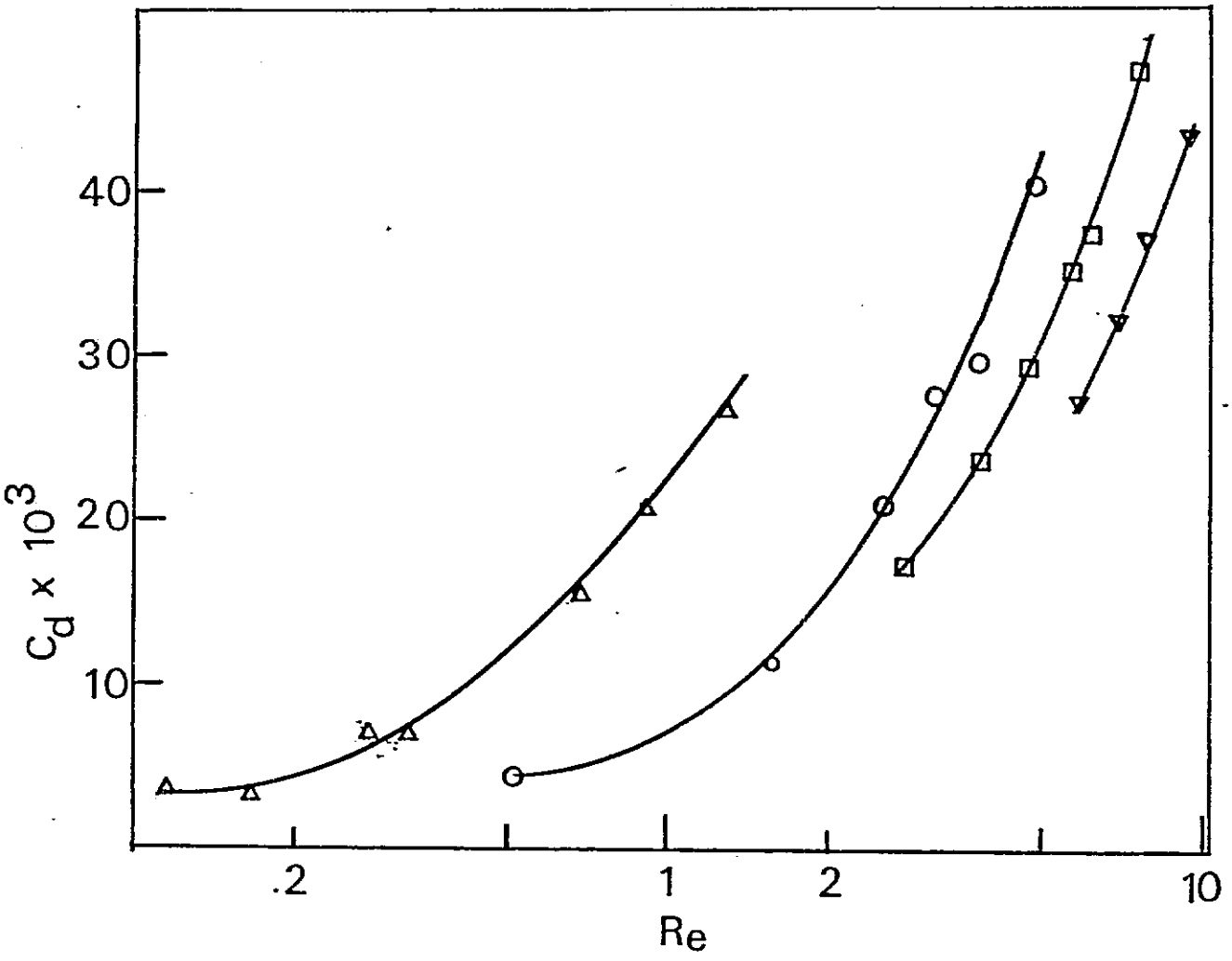

Figure 16. The discharge coefficient for the 15% CO_2 in air mixture flowing through the MCP as a function of Reynolds number. P_1 = Δ 4.39 torr, O 11.89 torr, □ 15.6 torr, ▽ 20.4 torr.

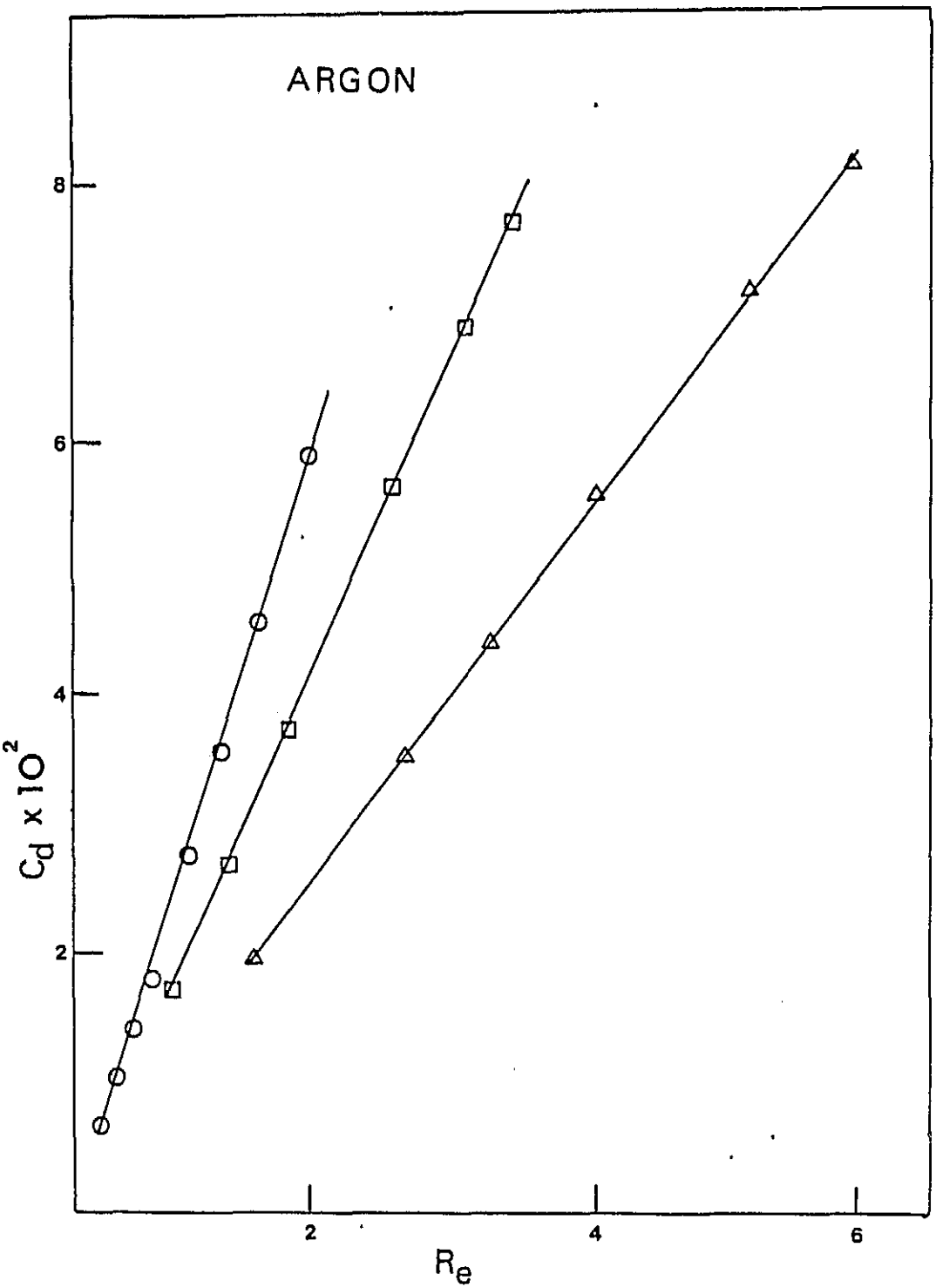

Figure 17. The discharge coefficient for the flow of Argon through the multi-channel plate as the Reynolds number is varied. P_1 = △ 13.7 torr, □ 8.27 torr, ○ 5.8 torr.

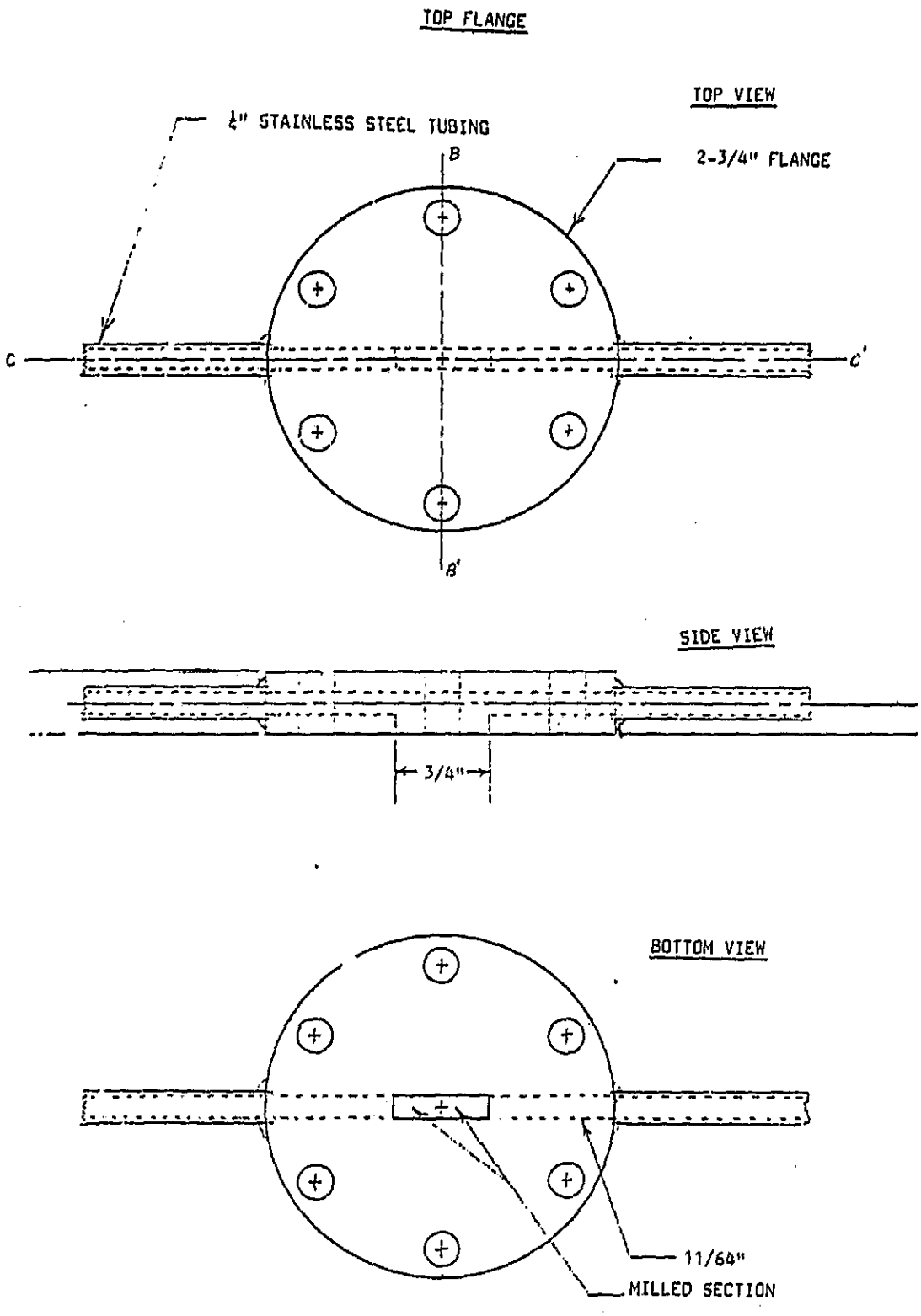

Figure 18a. Schematic for the top half of the flange containing the multi-channel plate for gas flow parallel to the surface of the plate.

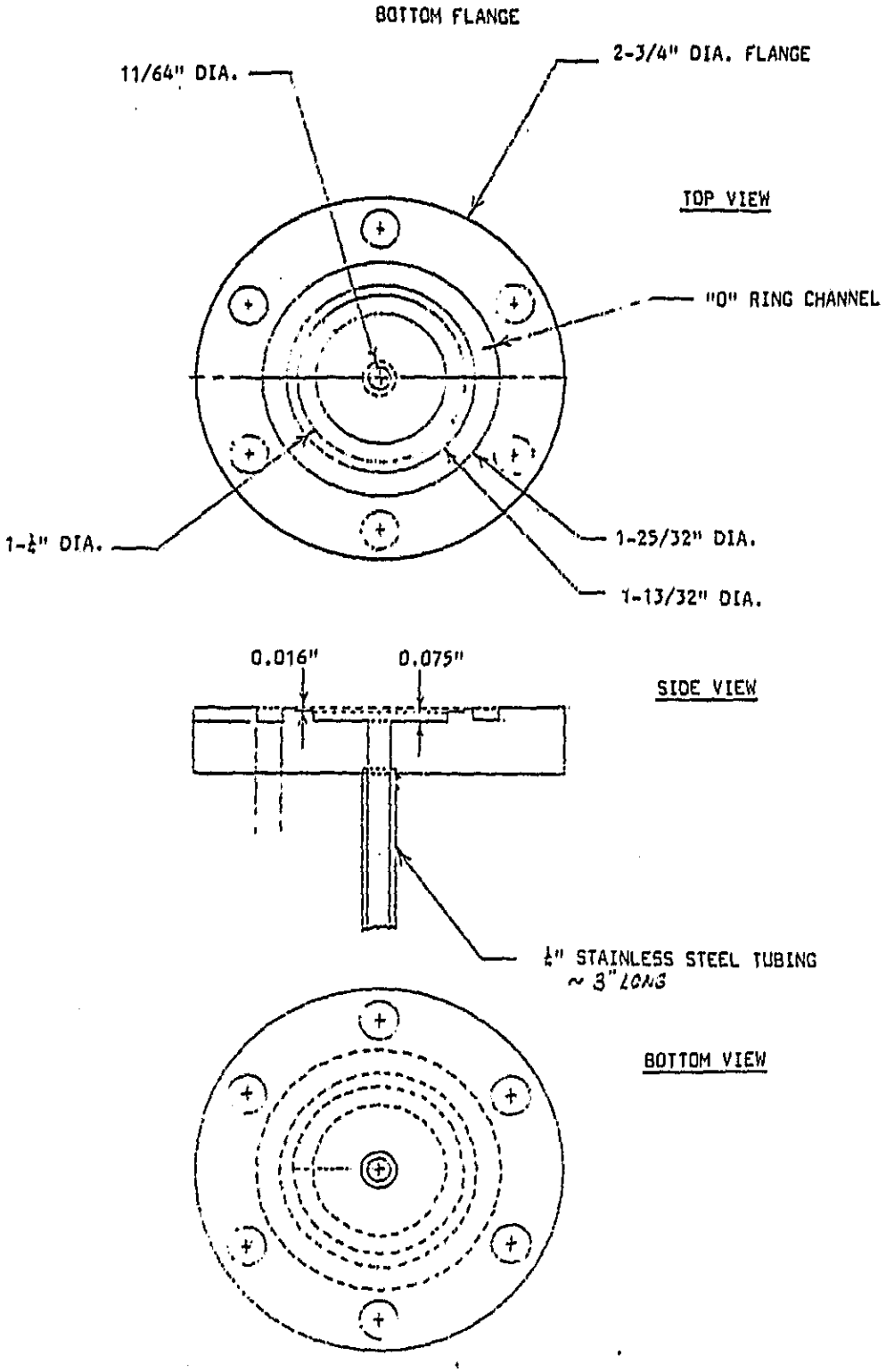

Figure 18b. A schematic for the bottom half of the parallel flow flange.

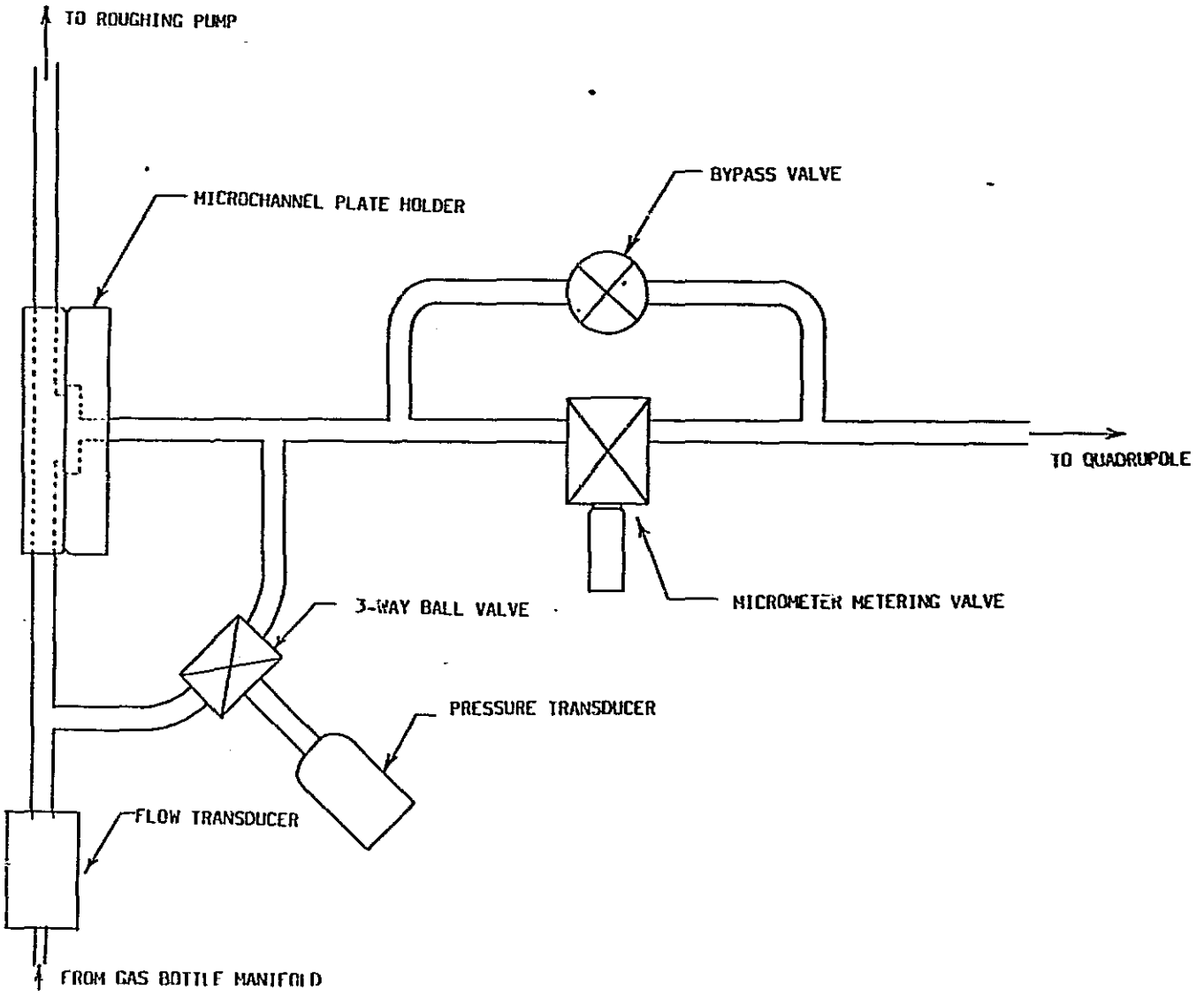

Figure 19. Schematic of the assembled apparatus for mass flow measurements and mass spectrometric measurements with the upstream flow parallel to the multichannel plate.

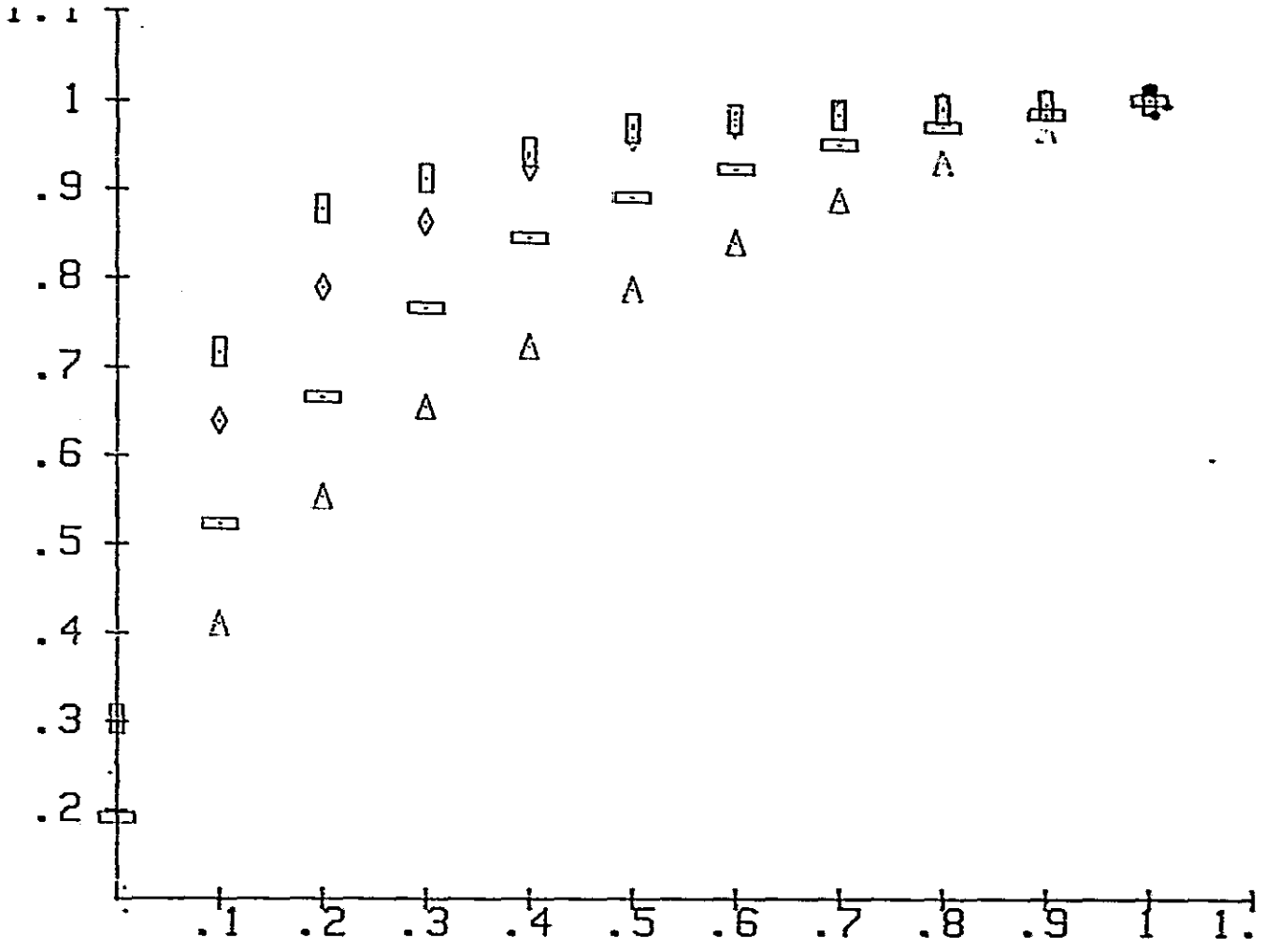

Figure 20. Temperature variation within the boundary layer at station 12 along the centerline. Temperature within the boundary layer is normalized by the temperature at the boundary layer at each altitude. The distance from the surface is normalized by the boundary layer thickness at each altitude. Relevant boundary layer parameters are found in Table VI. The free stream values are found in Table IV. The vehicle coordinates that correspond to the station position given in this figure and subsequent figures are described in Table V. □ 55 km, ◇ 65 km, ▭ 73 km, △ 84 km.

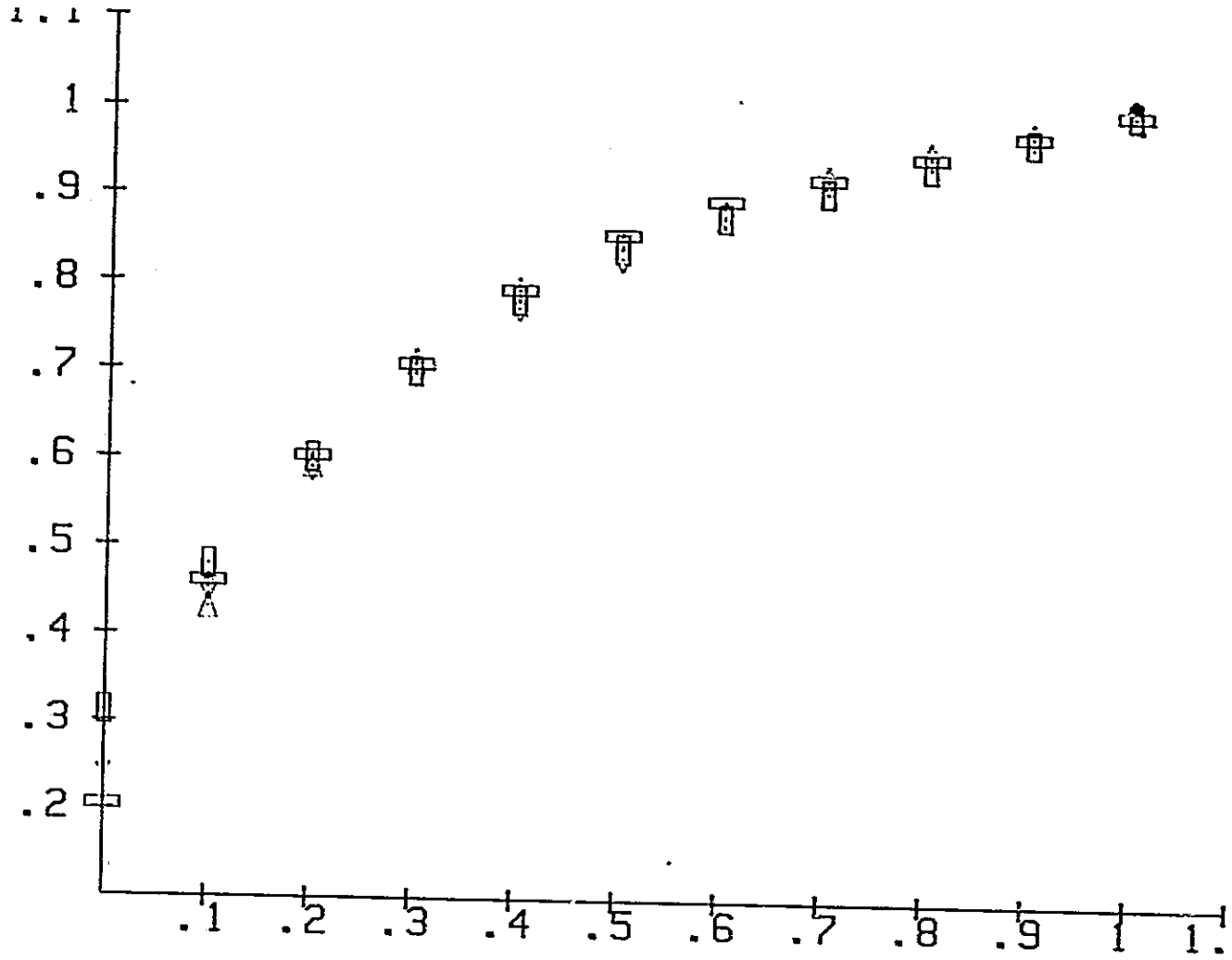

Figure 21. Temperature variation at station 24 downstream from station 12. See figure 20 for further description.

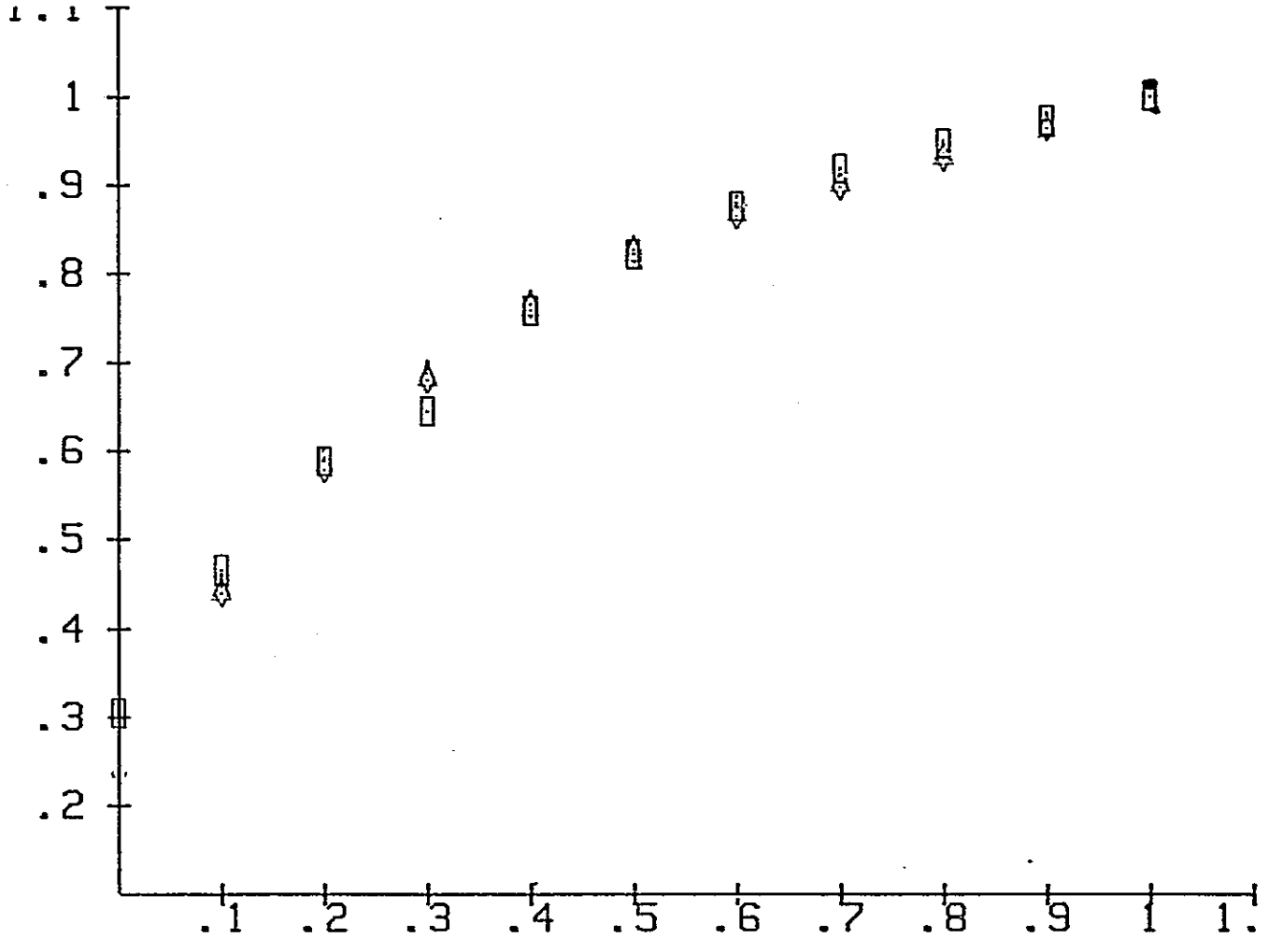

Figure 22. Temperature variation at station 30 downstream from station 24. See figure 20.

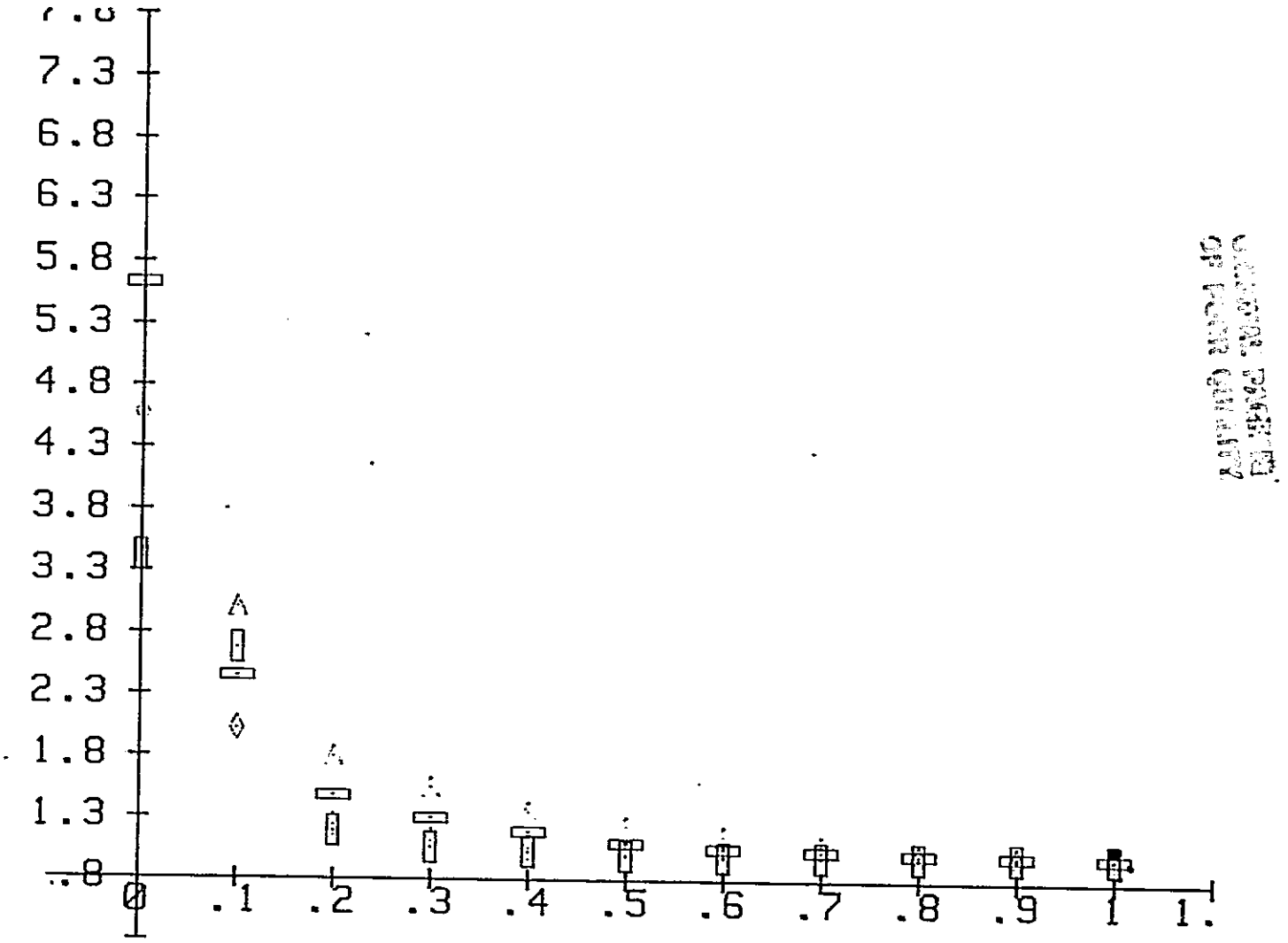

Figure 23. Density variaton within the boundary layer at station 12 on the centerline. The density is normalized by its value at the boundary layer. See figure 20 for further description.

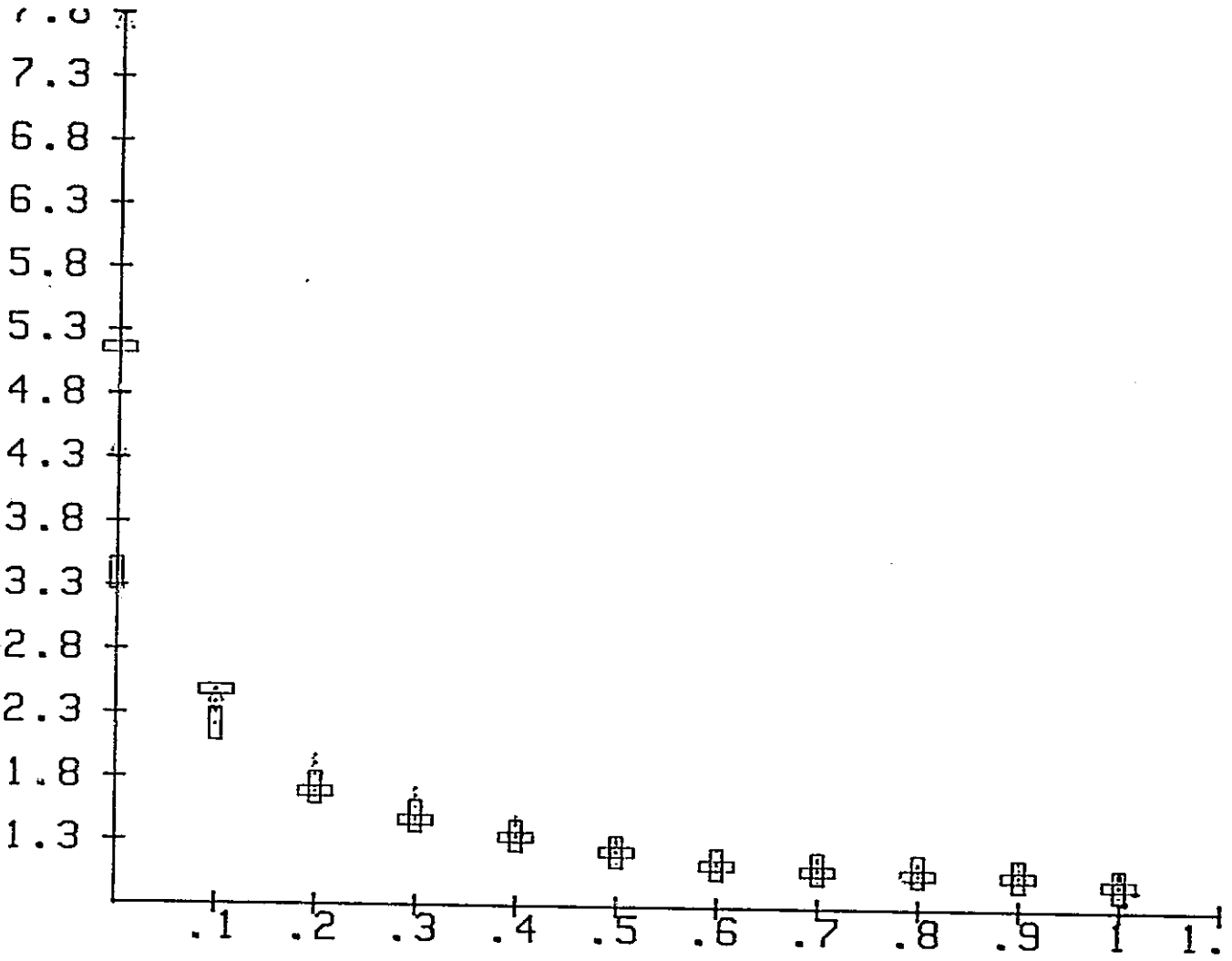

Figure 24. Density variation at station 24 downstream from station 12. See figure 20.

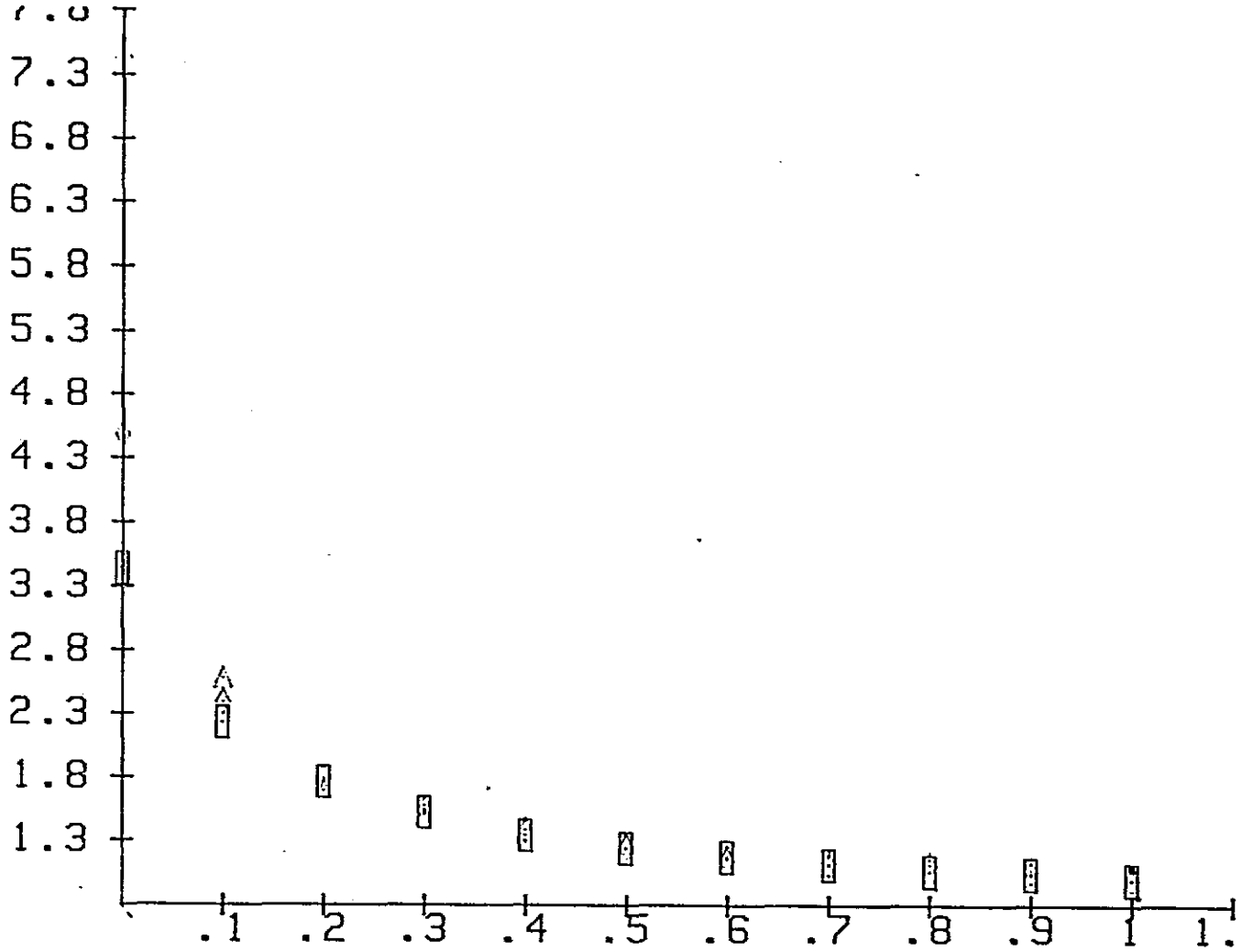

Figure 25. Density variation at station 30 downstream from station 24. See figure 20.

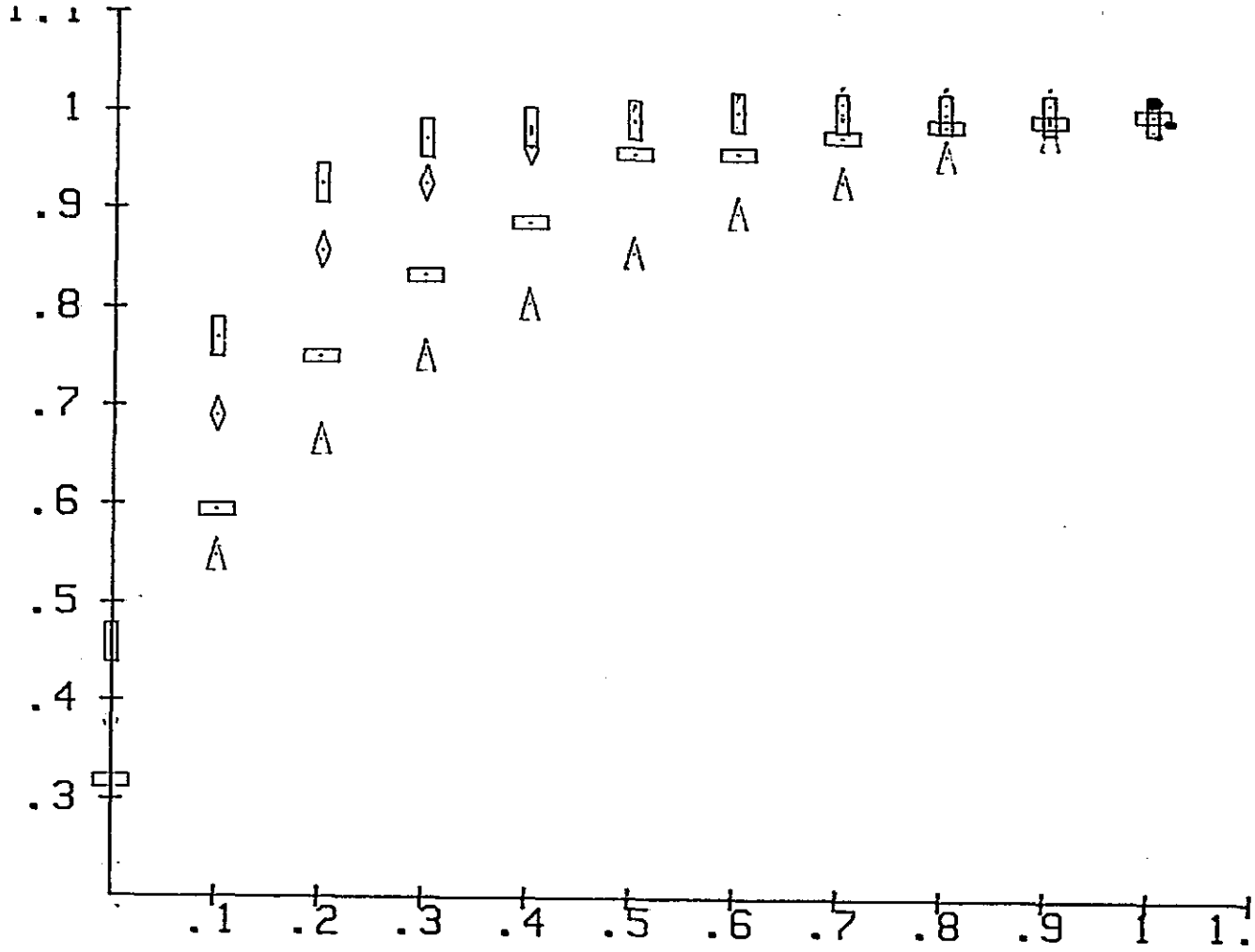

Figure 26. Viscosity variation within the boundary layer at station 12 along the centerline. The viscosity is normalized by its value at the boundary layer. For further description see Figure 20.

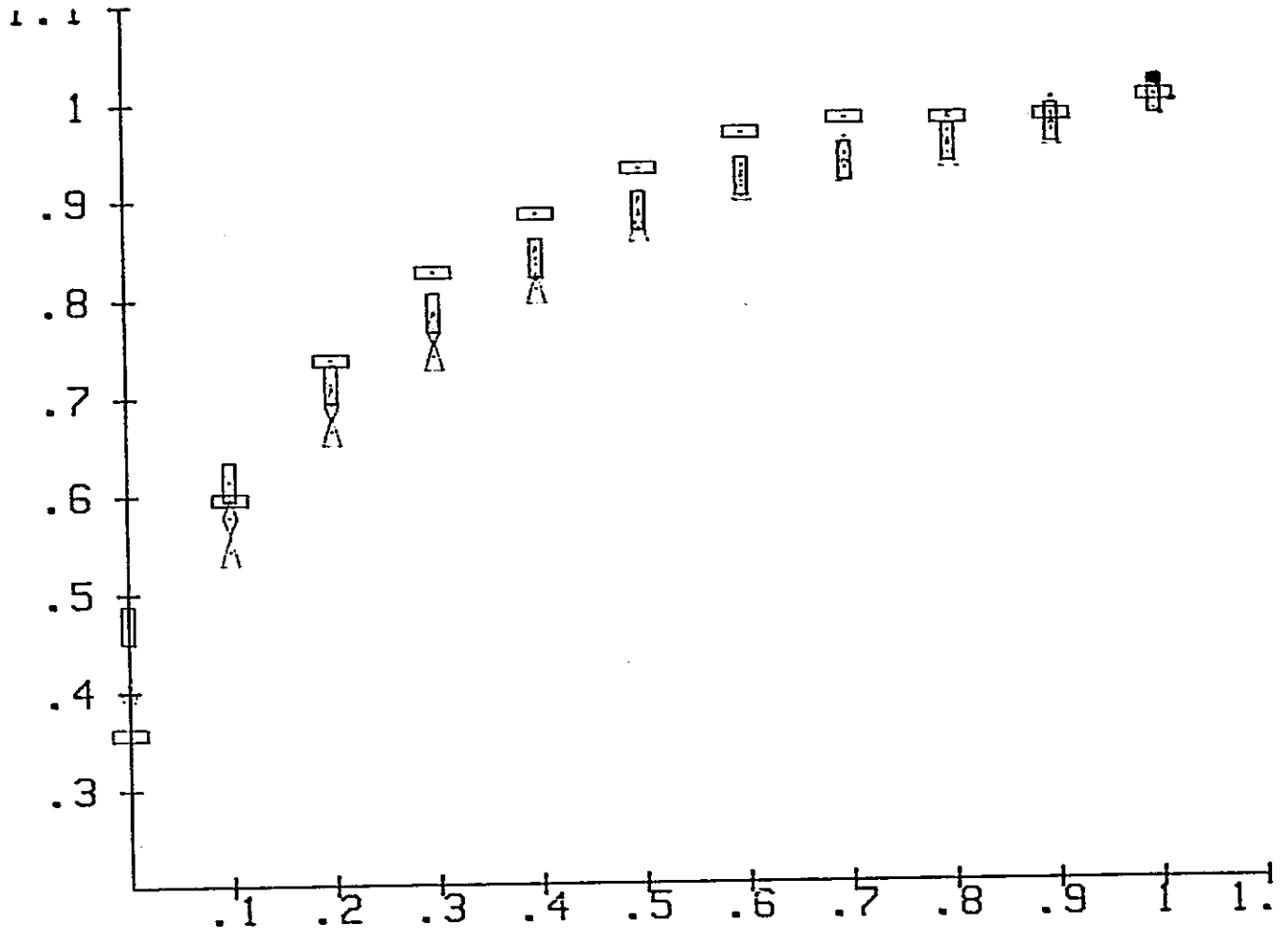

Figure 27. Viscosity at station 24 downstream from station 12. See figure 20.

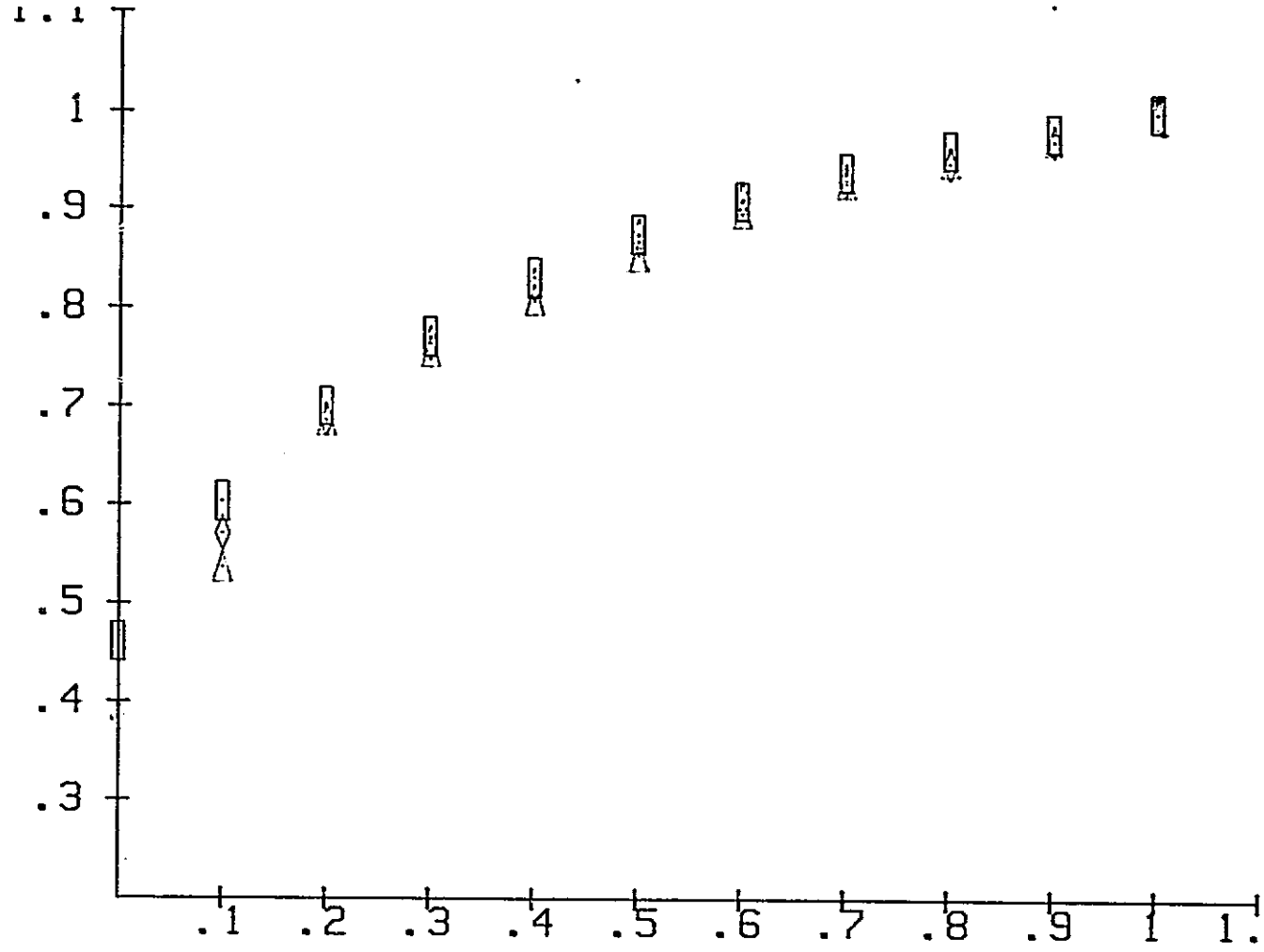

Figure 28. Viscosity at station 30 downstream from station 24. See figure 20.

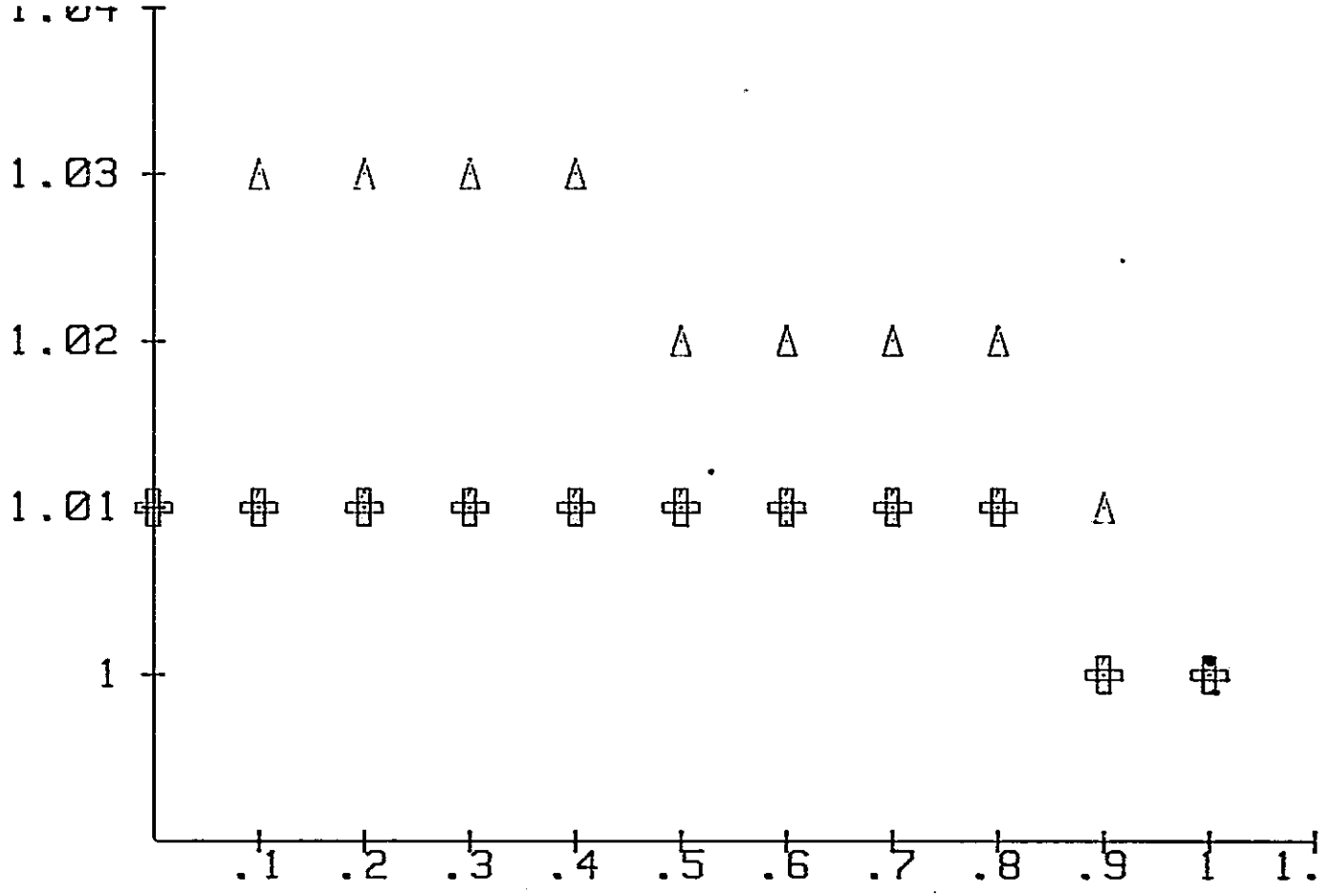

Figure 29. Pressure variation within the boundary layer at station 12 along the centerline. The pressure is normalized by its value at the boundary layer. See figure 20.

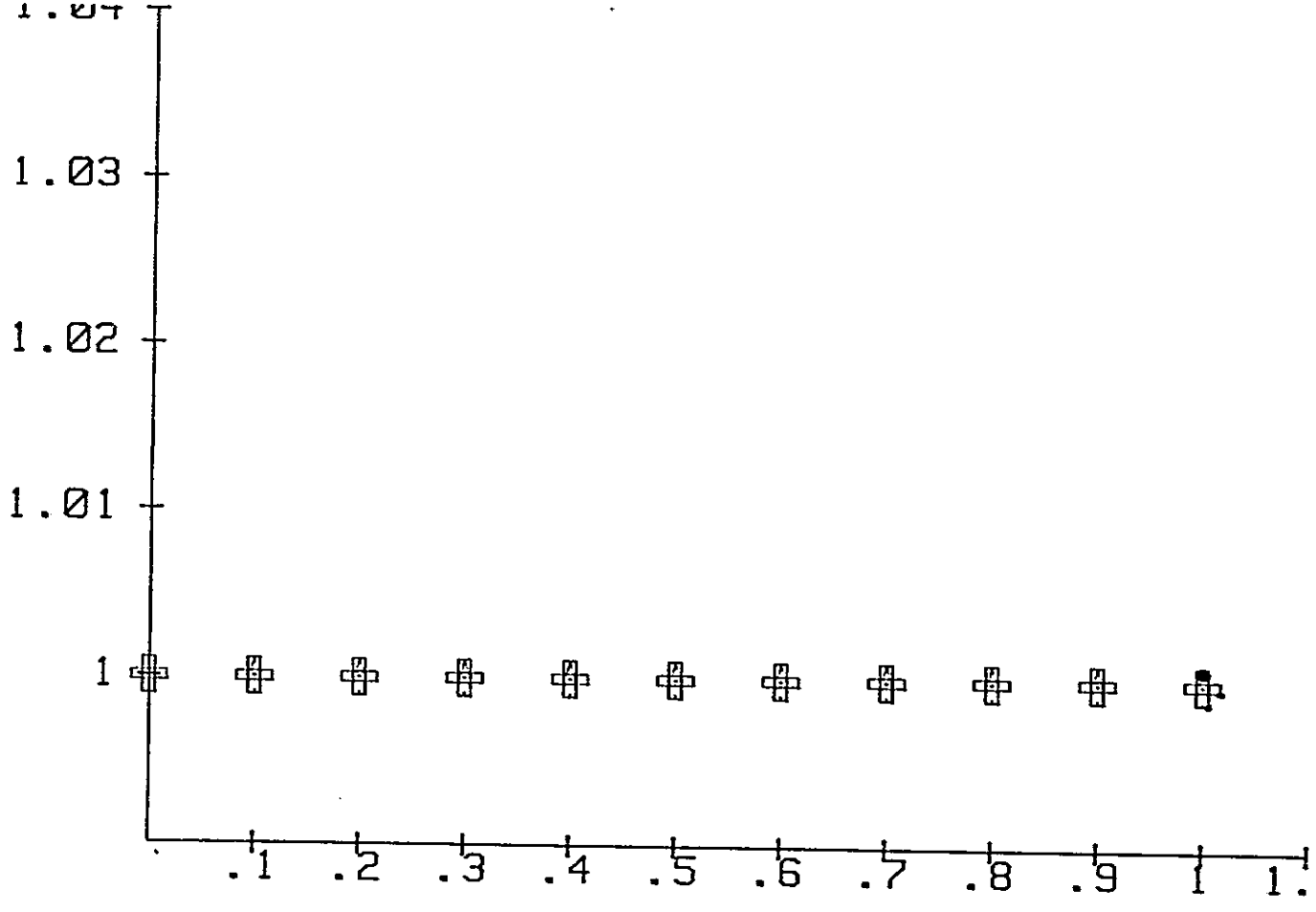

Figure 30. Pressure variation within the boundary layer at station 24 downstream from station 12. See figure 20.

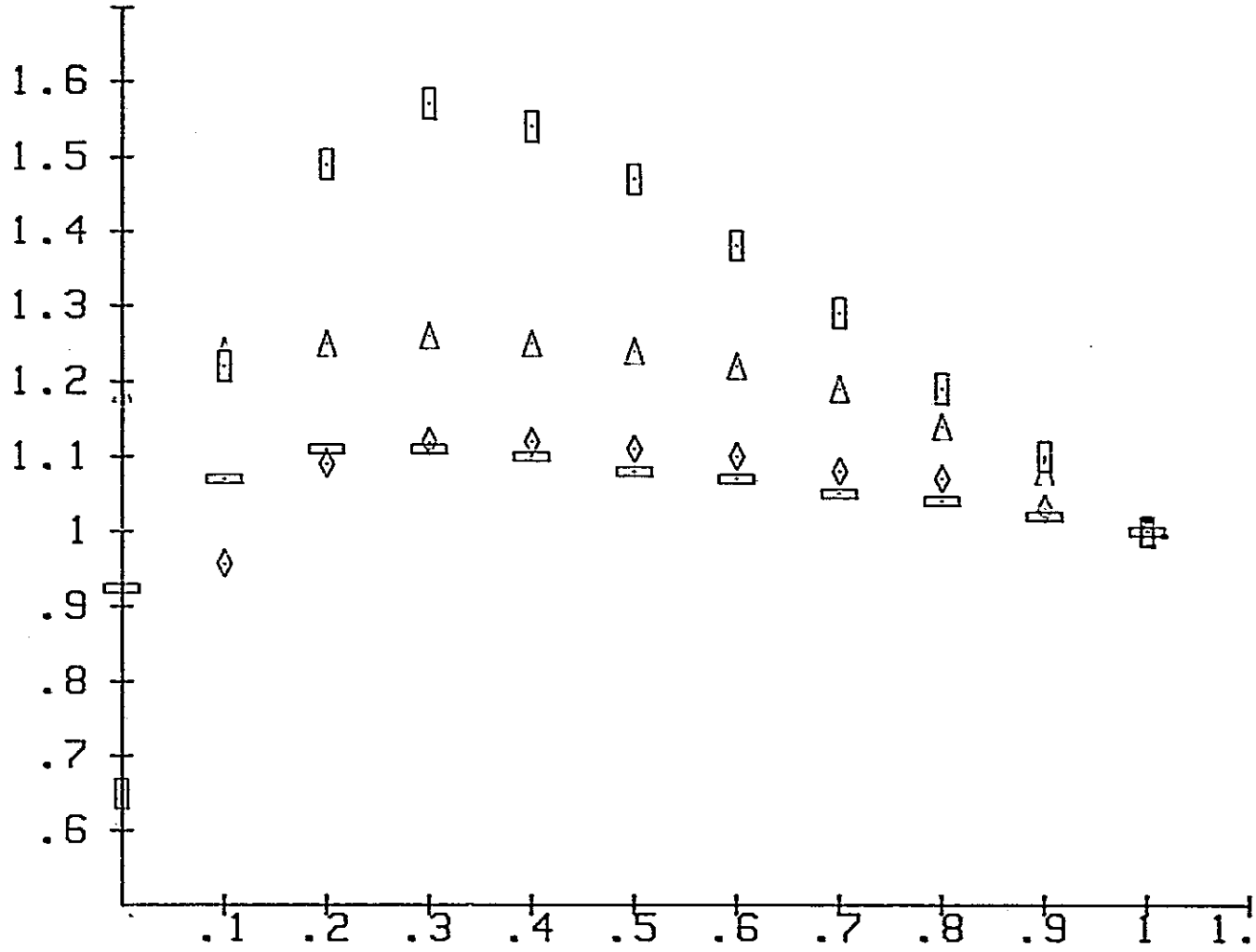

Figure 31. Variation of O atom mole fraction within the boundary layer at station 12 along the centerline. The O atom mole fraction is normalized by its value at the boundary layer. Boundary layer values for all species at all altitudes are shown in Tables VII-X. For further figure details see figure 20.

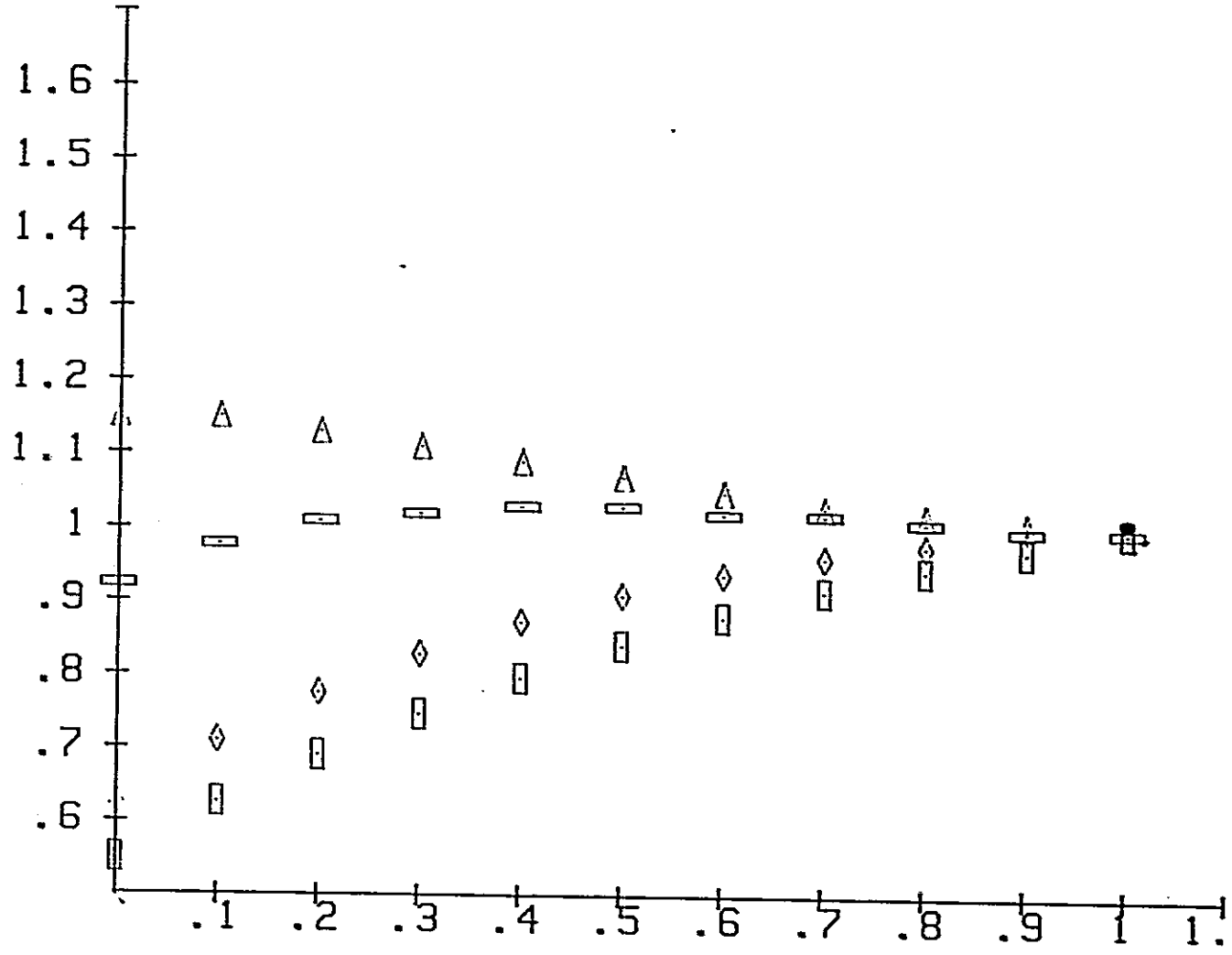

Figure 32. Variation of O atom mole fraction at station 24 downstream from station 12. See figure 31.

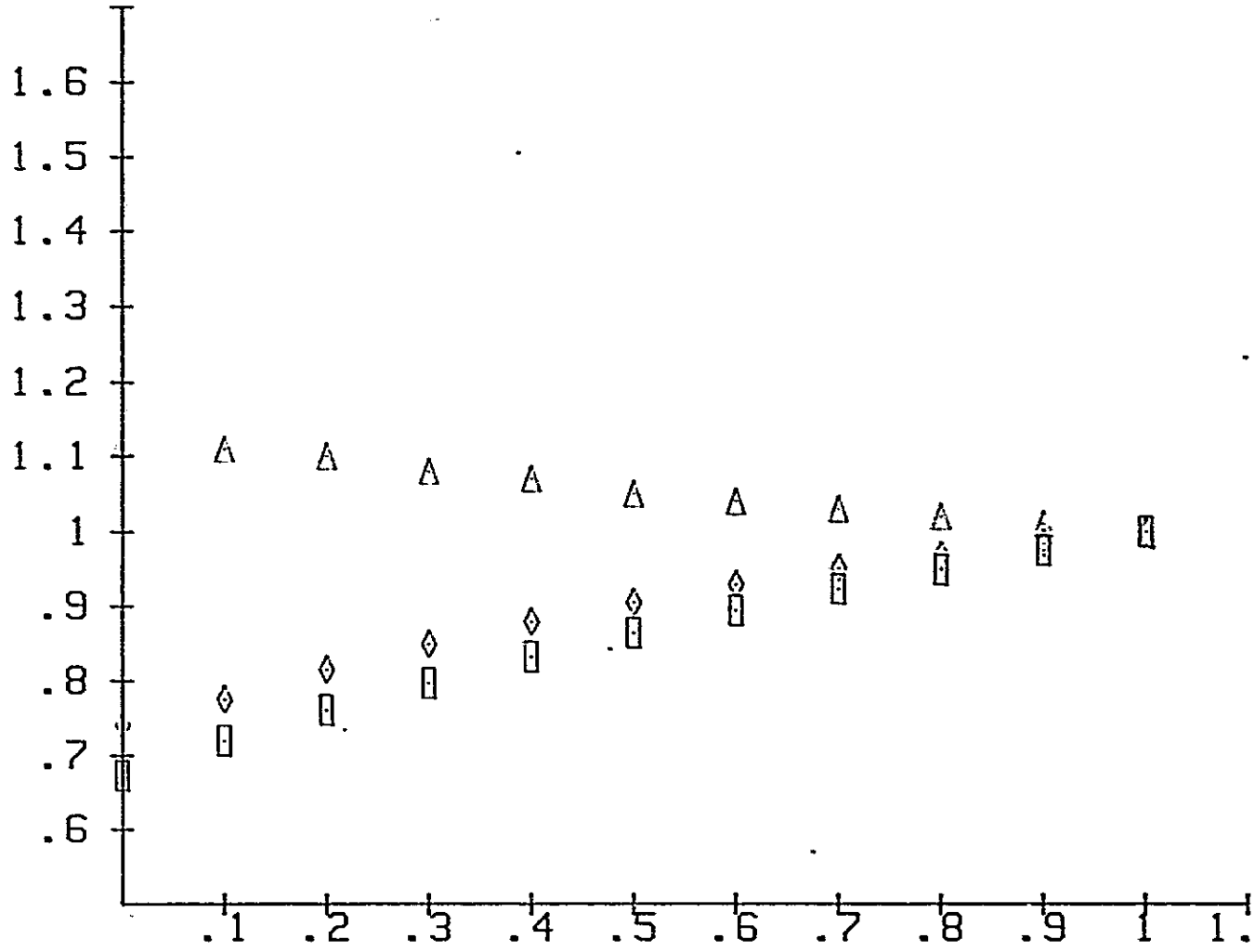

Figure 33. Variation of O atom mole fraction at station 30 downstream of station 12. See figure 31.

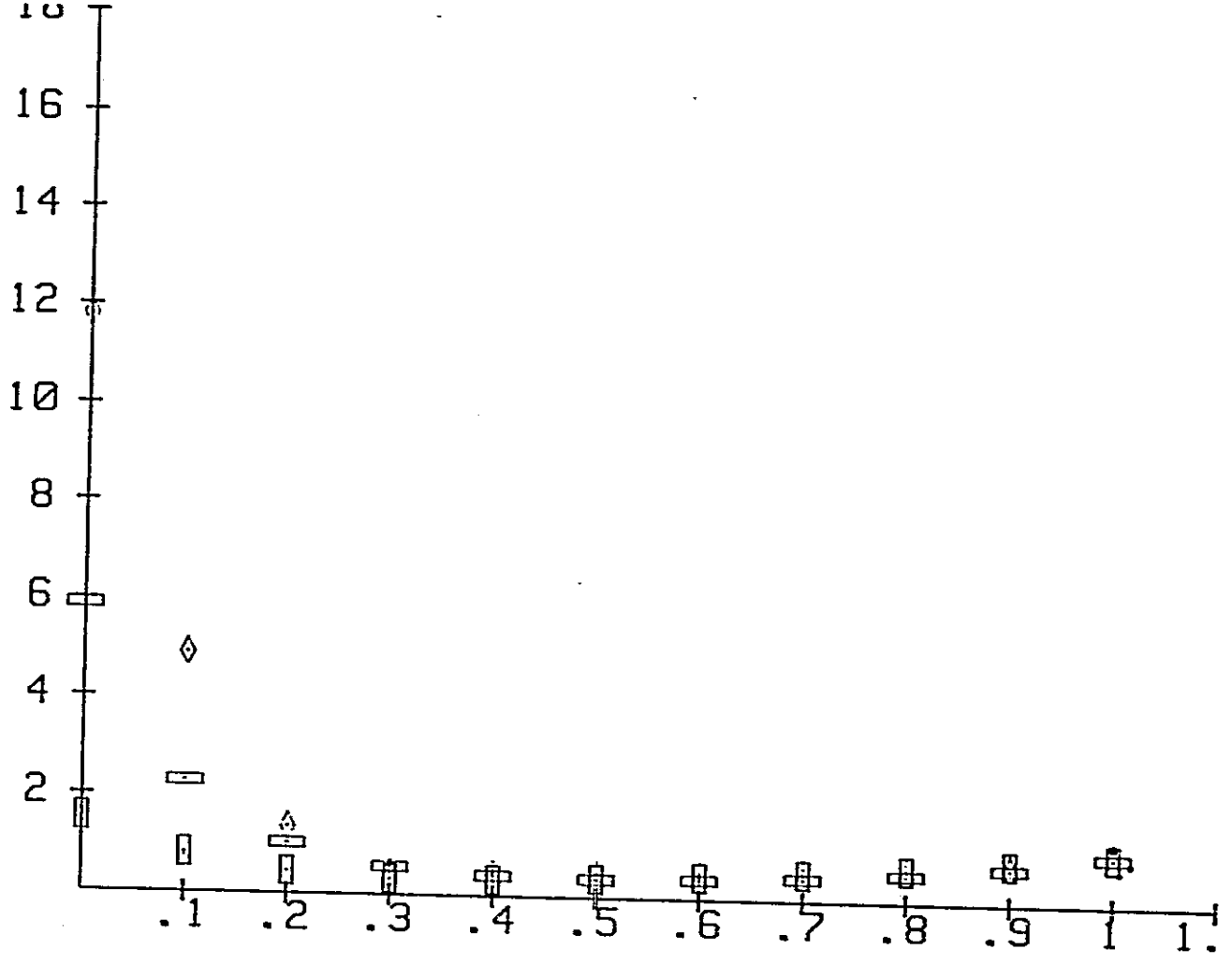

Figure 34. Variation of O_2 mole fraction within the boundary layer at station 12 along the centerline. The O_2 mole fraction is normalized by its value at the boundary layer. See figure 31.

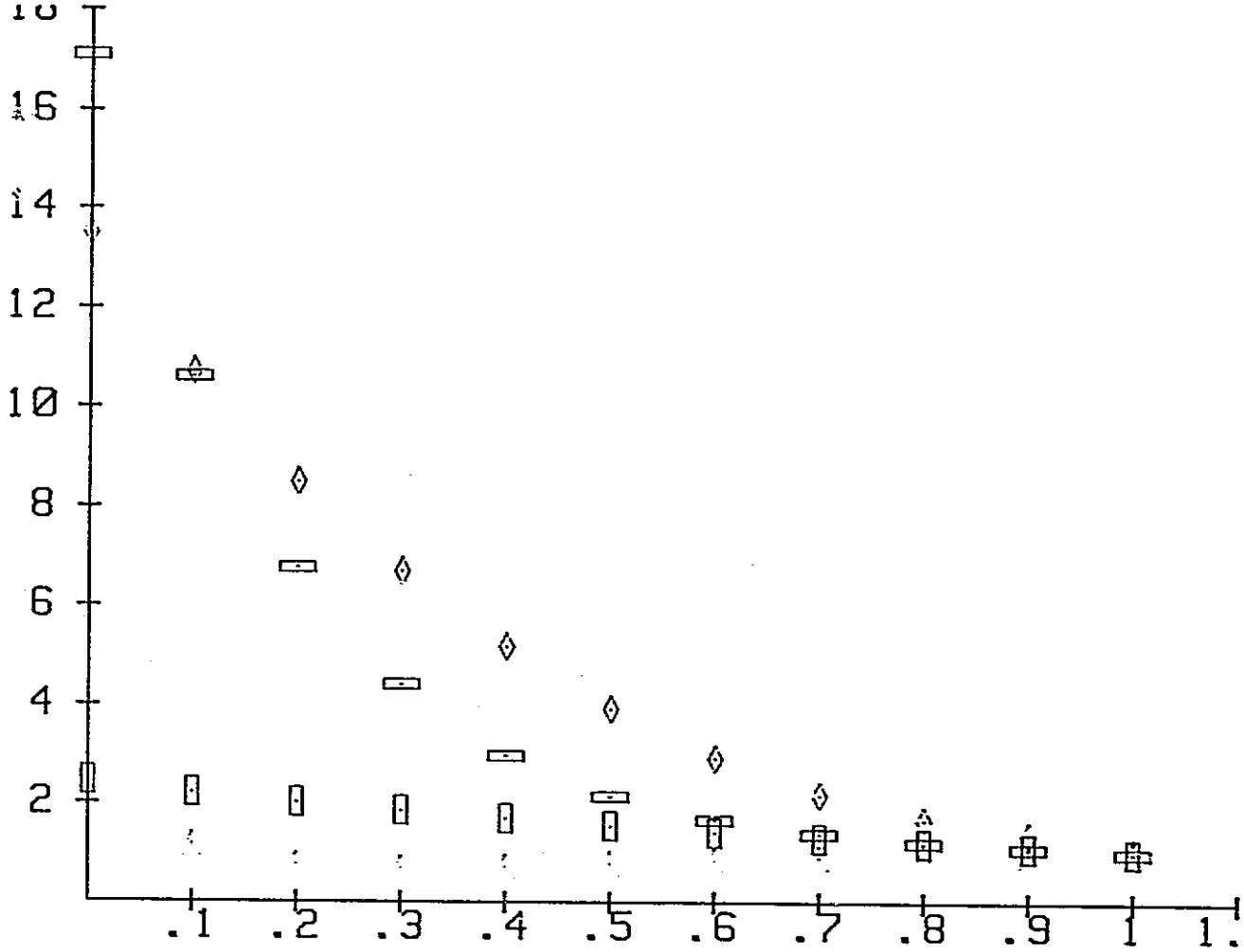

Figure 35. Variation of O_2 mole fraction at station 24 downstream of station 12. See figure 31.

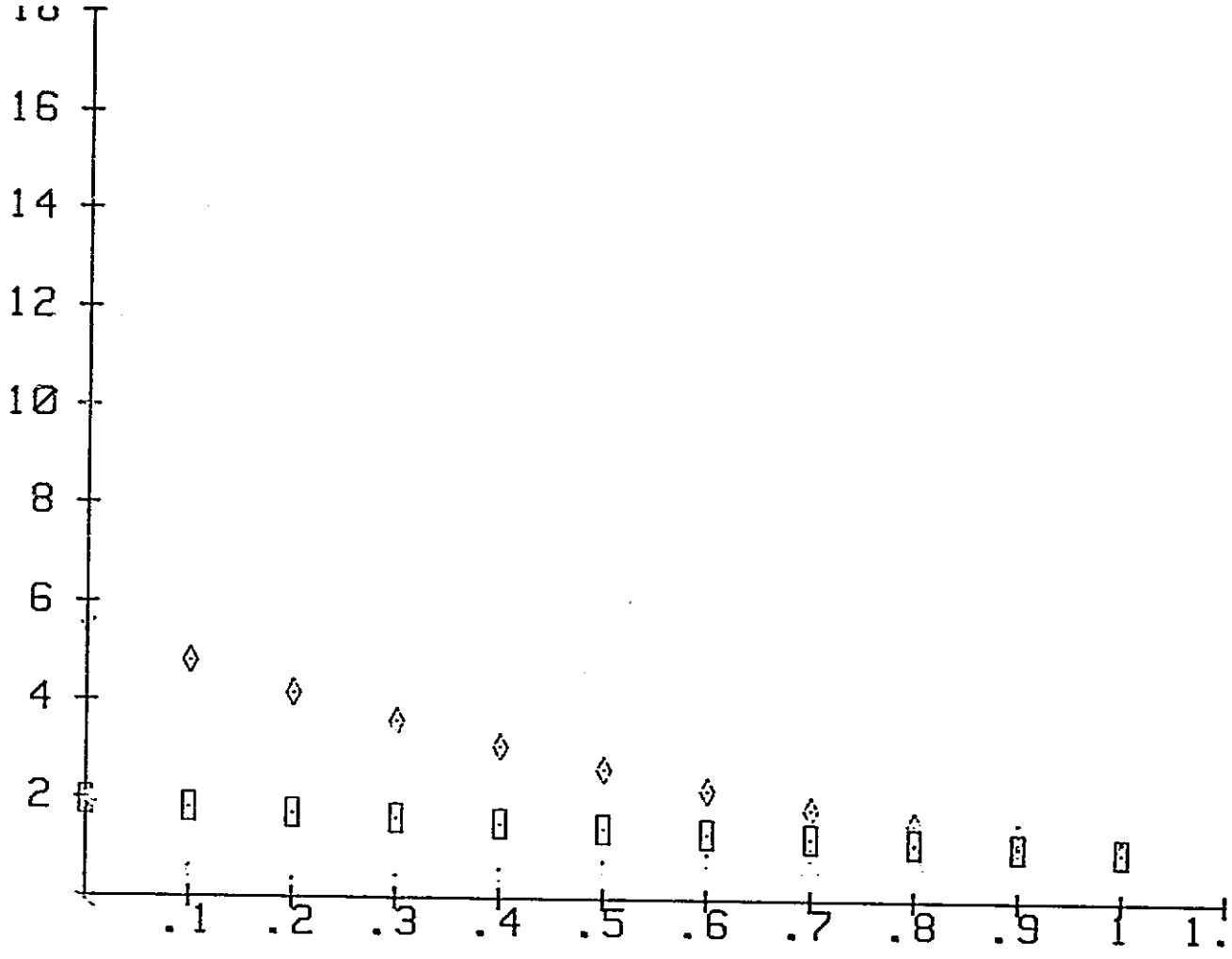

Figure 36. Variation of O_2 mole fraction at station 30 downstream of station 24. See figure 31.

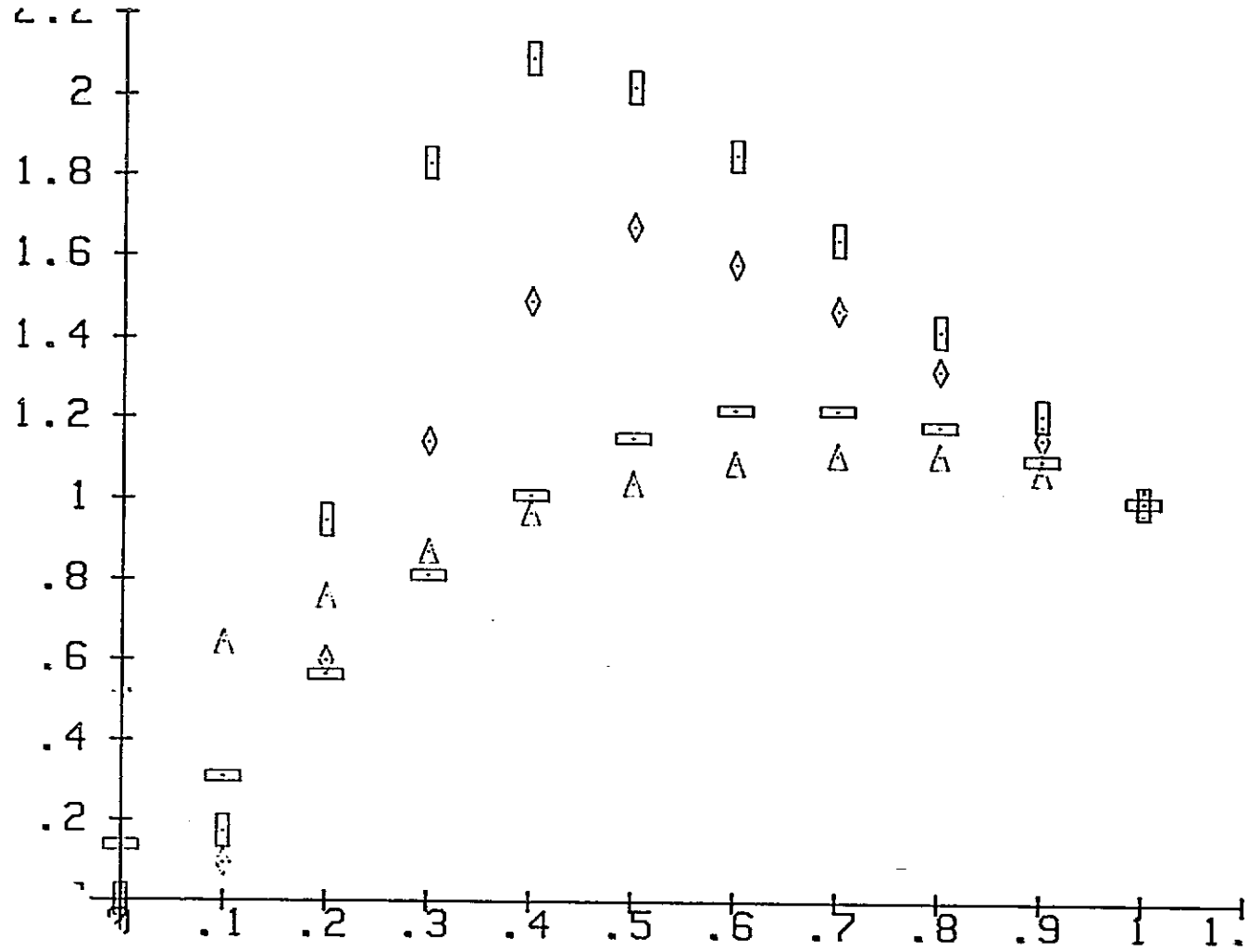

Figure 37. Variation of N atom mole fraction at station 12 along the centerline. The N atom mole fraction is normalized by its value at the boundary layer. See figure 31.

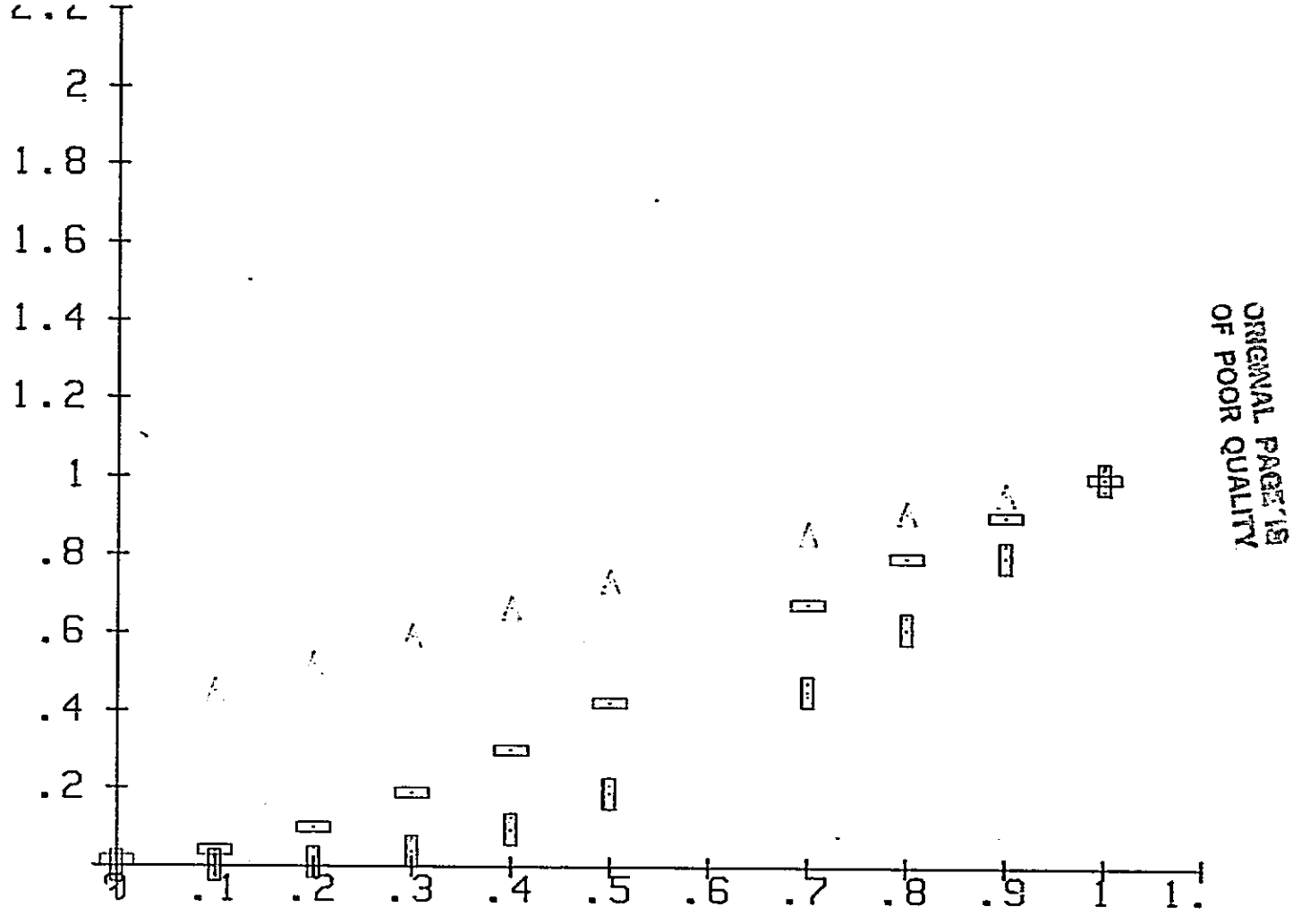

Figure 38. Variation of N atom mole fraction at station 24 downstream of station 12. See figure 31.

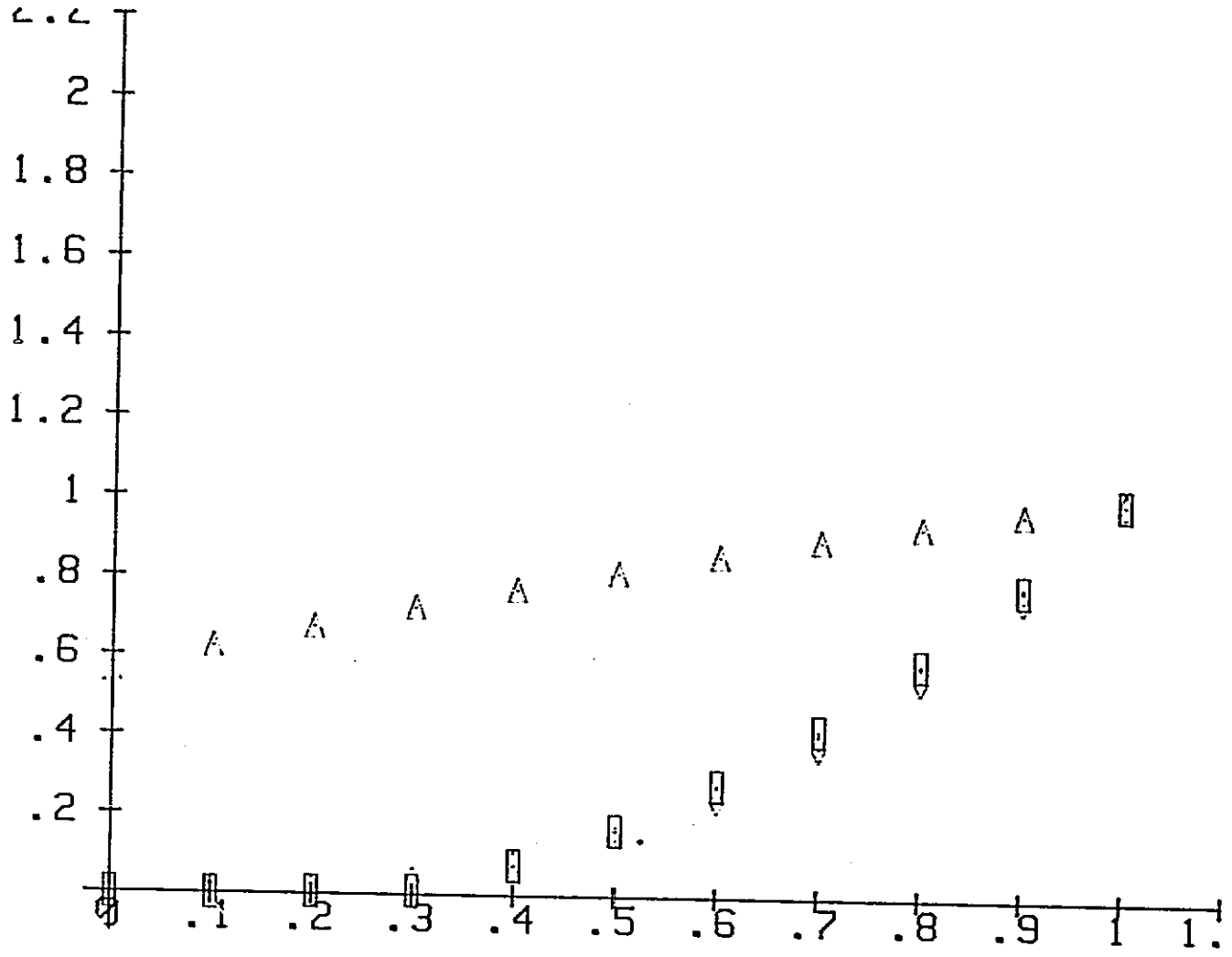

Figure 39. Variation of N atom mole fraction at station 30 downstream of station 24. See figure 31.

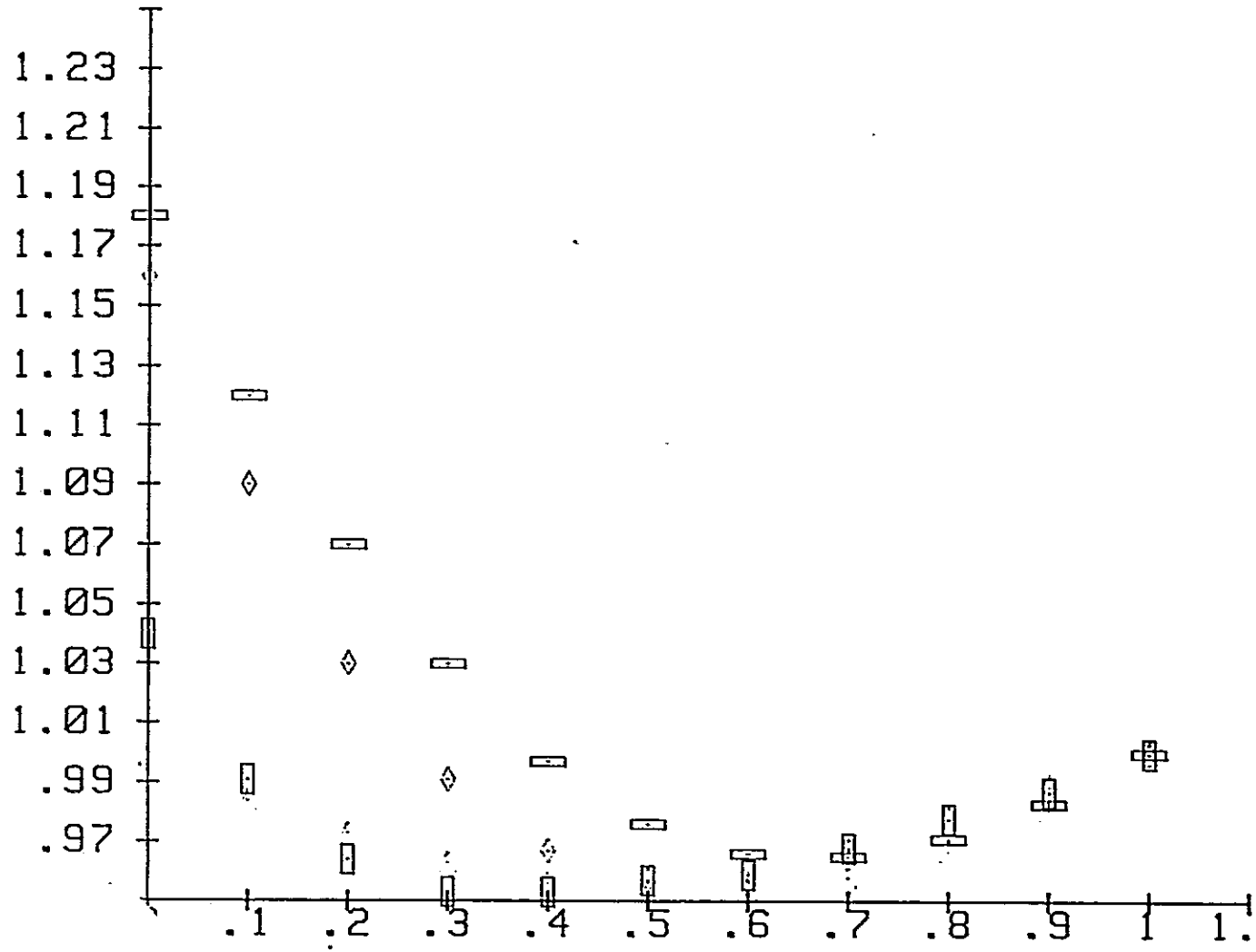

Figure 40. Variation of N_2 mole fraction within the boundary layer at station 12 along the centerline. The N_2 mole fraction is normalized by its value at the boundary layer. See figure 31.

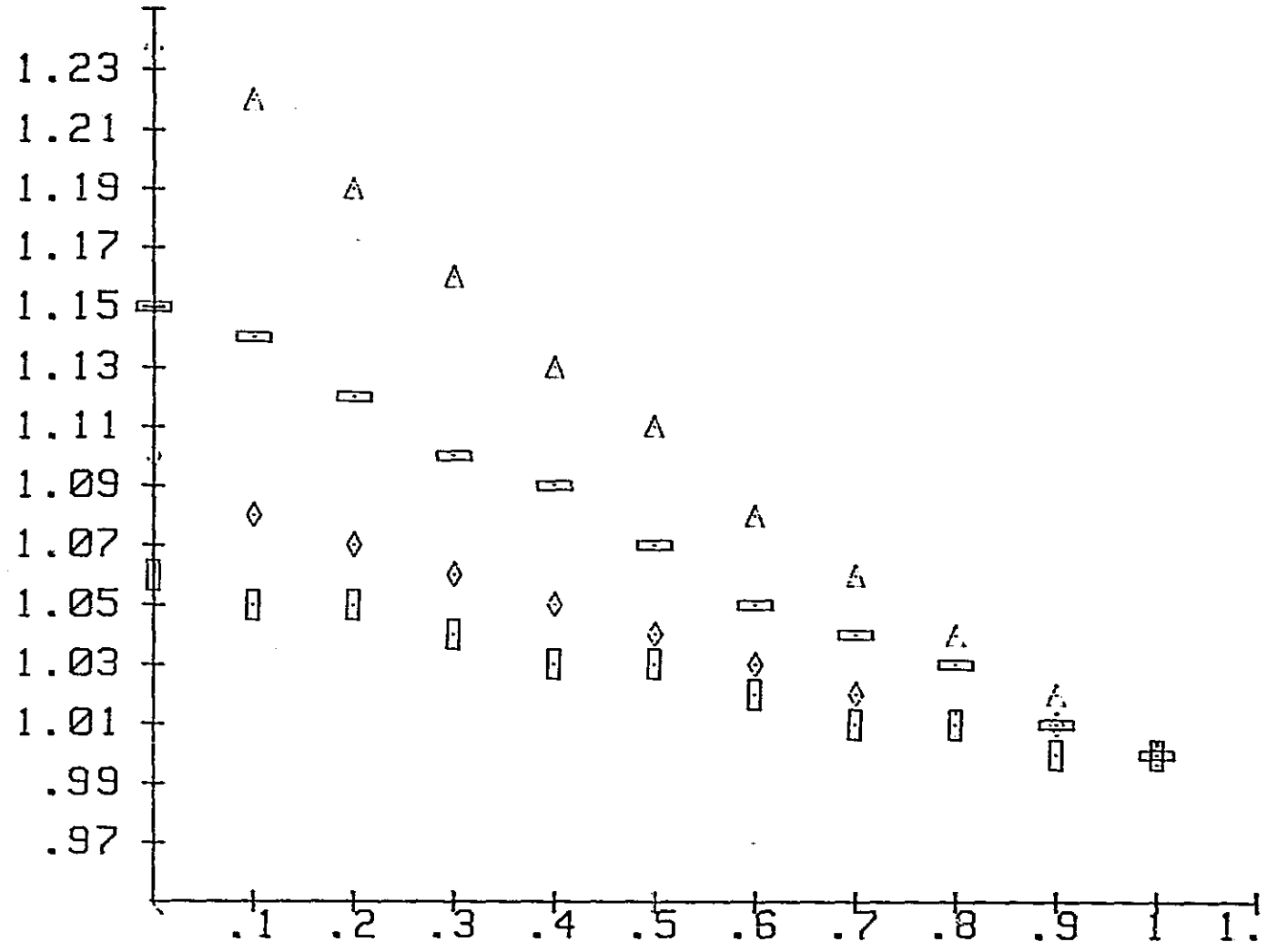

Figure 41. Variation of N_2 mole fraction within the boundary layer at station 24 downstream from station 12. See figure 31.

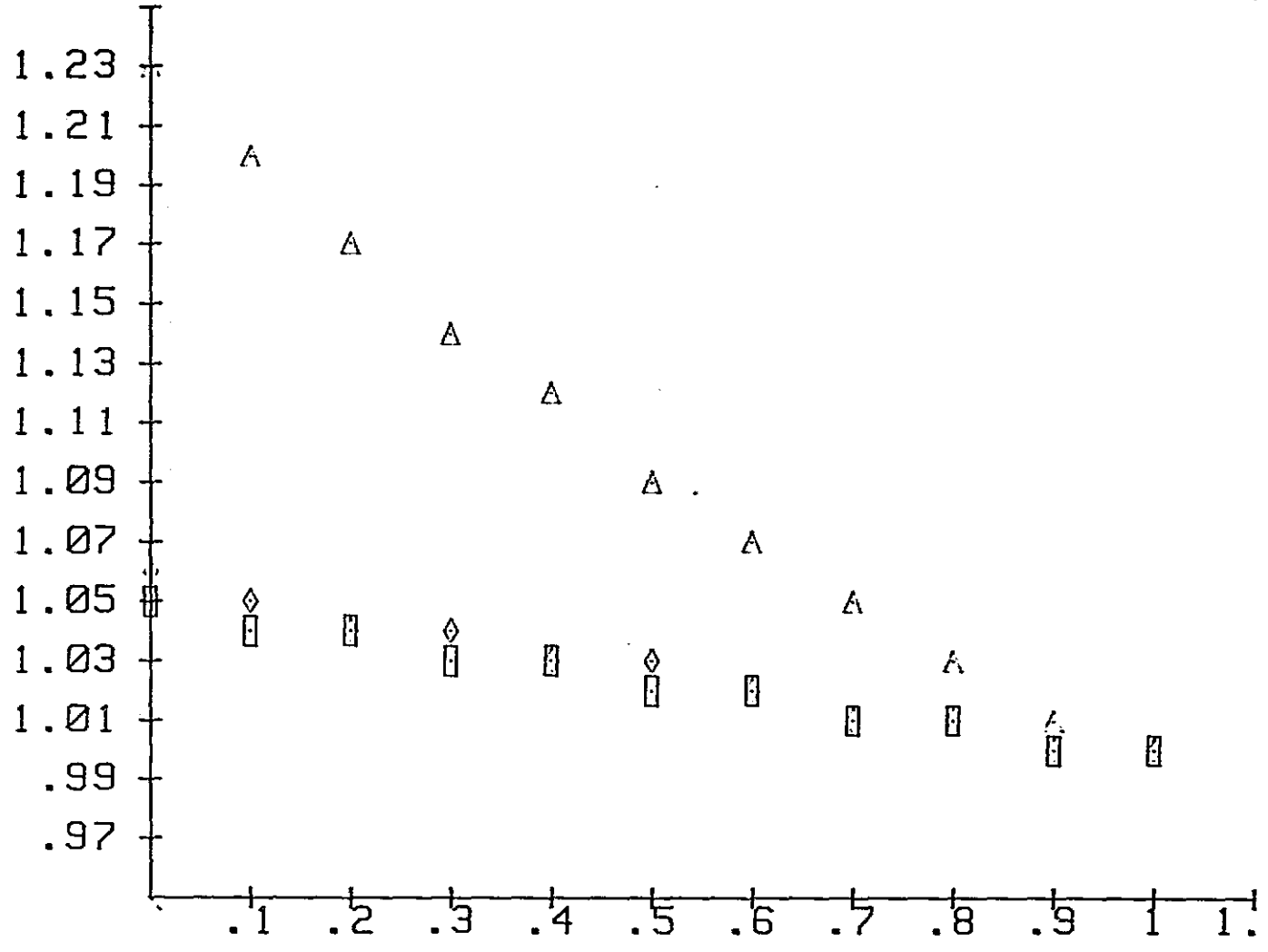

Figure 42. Variation of N_2 mole fraction within the boundary layer at station 32 downstream from station 24. See figure 31.

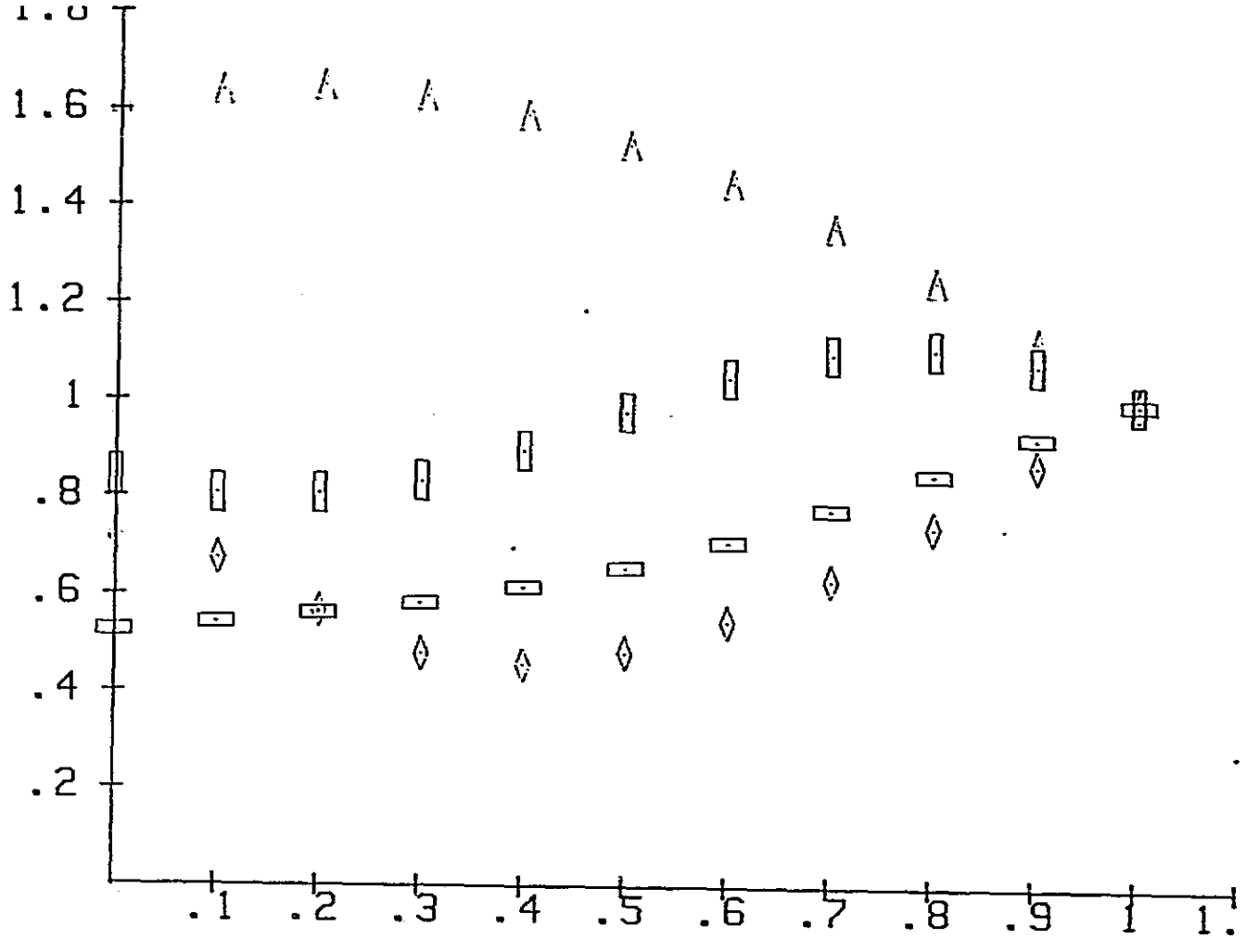

Figure 43. Variation of NO within the boundary layer at station 12 along the centerline. The NO mole fraction is normalized by its value at the boundary layer. See figure 31.

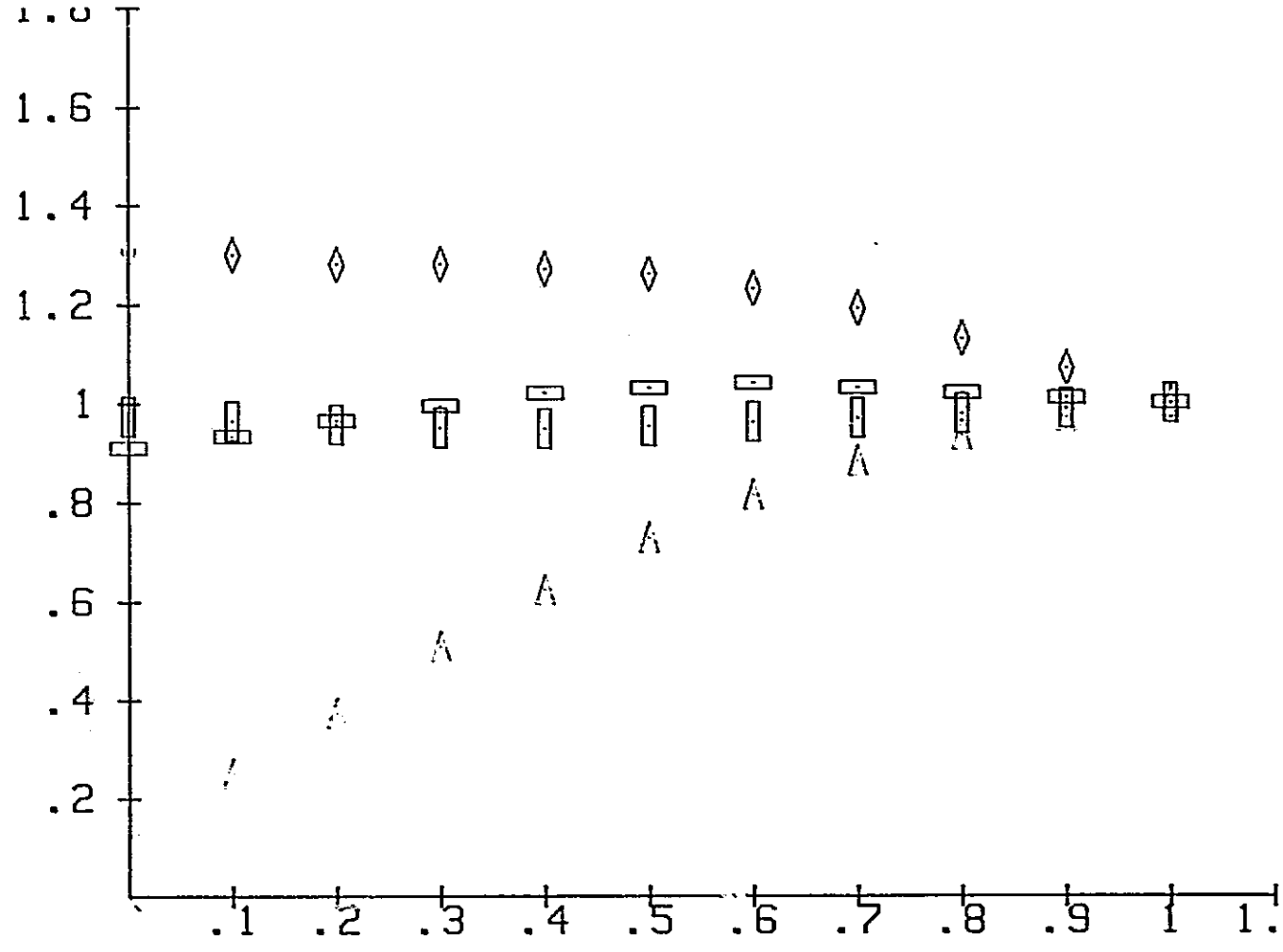

Figure 44. Variation of NO mole fraction at station 24 downstream from station 12. See figure 31.

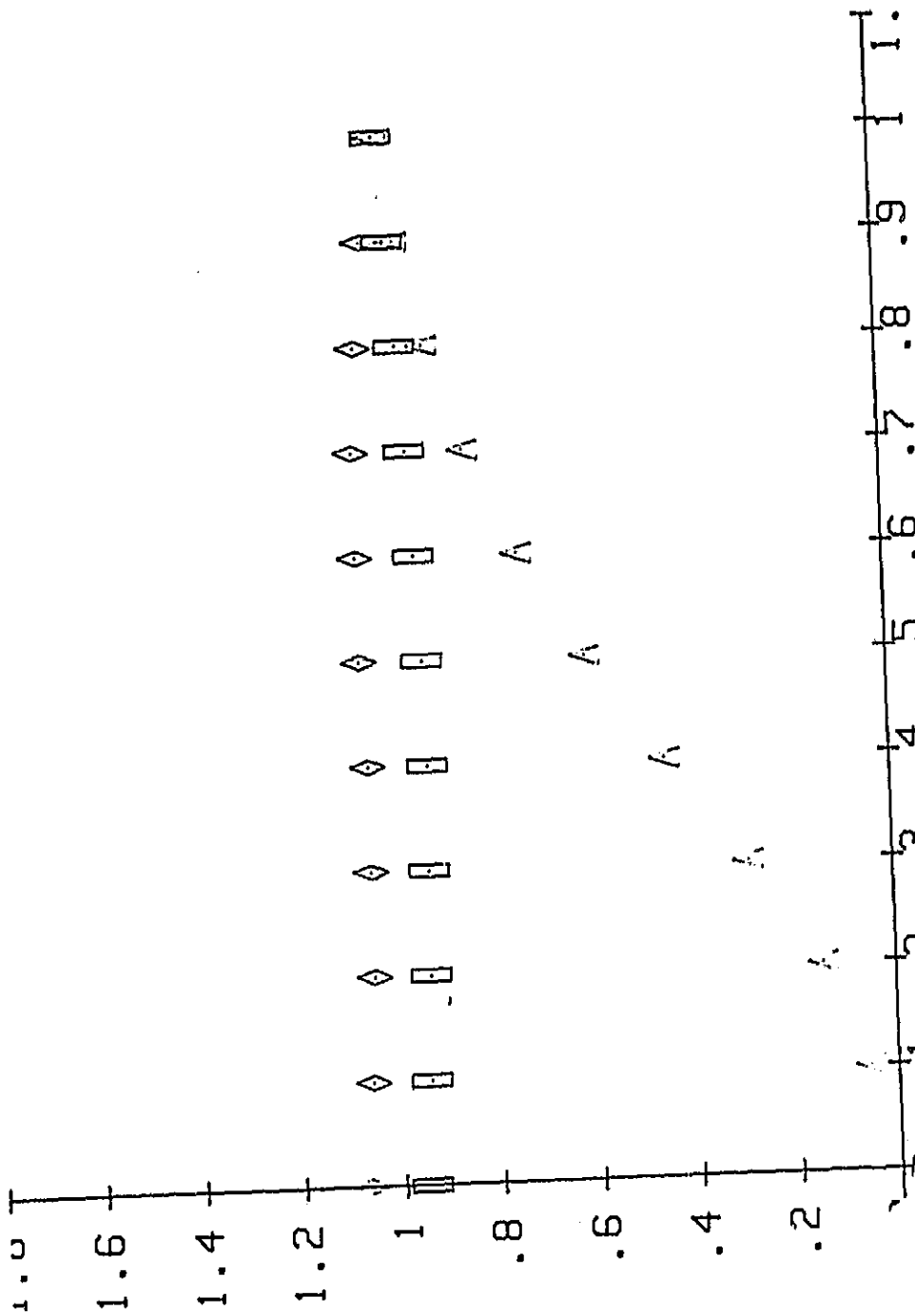

Figure 45. Variation of NO mole fraction at station 30 downstream from station 24. See figure 31.